Physics – Uspekhi **53** (10) 995 – 1014 (2010)

REVIEWS OF TOPICAL PROBLEMS PACS numbers: 68.03.Hj, 68.35.B –, 68.35.Fx, **68.37. – d**, **73.20. – r**, **79.60. – i**

Oxide nanostructures on an Nb surface and related systems: experiments and *ab initio* calculations

M V Kuznetsov, A S Razinkin, A L Ivanovskii

DOI: 10.3367/UFNe.0180.201010b.1035

Contents

Abstract. This review discusses the state of the art in two related research areas: the surfaces of niobium and of its related group IV–VI transition metals, and surface (primarily oxide) nanostructures that form on niobium (and group IV–VI d-metals) due to gas adsorption or impurity diffusion from the bulk. Experimental (X-ray photoelectron spectroscopy, photoelectron diffraction, scanning tunneling microscopy) and theoretical (*ab initio* simulation) results on d-metal surfaces are summarized and reviewed.

1. Introduction

The question of the self-organization of atoms on the surface of crystals and of the initial stages of phase formation are among the key issues in modern physics and physical materials science, being fundamental for the creation of surface nanostructures for electronics and photonics, the deposition of thin films and coatings, heterogeneous catalysis, etc. The obvious success in studying crystal surfaces is mainly related to the development of physical techniques of surface analysis and correct theoretical methods for the simulation of surface characteristics. The combined use of these approaches makes it possible to obtain detailed information on the morphology and structure of the surface, localization of adsorbed atoms and molecules, electronic structure, and nature of interatomic interactions in the subsurface region and on the surface.

M V Kuznetsov, A S Razinkin, A L Ivanovskii Institute of Solid State Chemistry, Ural Branch of the Russian Academy of Sciences, ul. Pervomaiskaya 91, 640041 Ekaterinburg, Russian Federation
Tel. (7-343) 362 33 56. Fax (7-343) 374 44 95
E-mail: kuznetsov@ihim.uran.ru

Received 15 March 2010
Uspekhi Fizicheskikh Nauk **180** (10) 1035 – 1054 (2010)
DOI: 10.3367/UFNr.0180.201010b.1035
Translated by S N Gorin; edited by A Radzig

At present, great attention is being paid to the development of methods for the creation of new surface nanostructures with desired functional characteristics. The circle of research objects is expanding substantially; more and more complex systems, which are characterized by a large variety of processes occurring on the surface, are involved in the consideration.

Among such systems attracting considerable attention are group IV–VI d-metal surfaces on which there occur, simultaneously and concordantly, processes such as the dissociative chemisorption of an adsorbate, diffusion of adatoms into the bulk of the metal or, on the contrary, segregation of atoms from the bulk to the surface, formation of new structures on the surface, and so forth.

In turn, niobium, as well as its alloys and compounds, is of greatest interest among the d-metals primarily due to their superconducting properties. For example, niobium is applied for producing superconducting resonators in the accelerators of elementary particles [1]. Niobium films are used in magnetic-field sensors based on the Josephson effect [2]. Recently, the creation of a superconducting detector based on NbN monolayers, capable of detecting individual photons of infrared radiation, was reported, whose sensitivity and operation speed are the thousand times greater (are equal to several gigahertz) than those of the available semiconductor detectors [3]. Various ways are being considered of creating new niobium-compound-based memory devices using single-electron transistors and rapid single-flux quantum logic [4, 5]. All these devices are based on Nb or NbN films, namely, on very thin and maximally pure layers. The problem, however, is that it is very difficult to obtain 'pure' niobium films, since even niobium layers deposited at a vacuum level of $\sim 10^{-8}$ Pa contain specific oxide structures on their surfaces. What do these structures represent, and what is their composition, chemical nature, atomic topology, and properties? How can one avoid the formation of such structures or, on the contrary, use them for practical purposes?

In this review we shall attempt to generalize the modern state of investigations of the pure niobium surface and of surface (mainly oxide) nanostructures that are formed on niobium due to the adsorption of gases from the gaseous phase or due to the diffusion of impurities from the bulk of the metal. These results are compared with the available data for related systems—surface nanostructures on group IV–VI d-metals. The low dimensionality of these structures determines the unique techniques for their preparation and investigation. Therefore, the main focus is on the results of an analysis of the surface of the above-mentioned systems by the methods of X-ray photoelectron spectroscopy (XPS), X-ray photoelectron diffraction (XPD) [8–10], and scanning tunneling microscopy (STM) [11, 12], as well as by the computational *ab initio* methods of the energy-band theory of the condensed state, which proved to be efficient in solving the above-mentioned problems and are widely applied in the current practice of such studies.

2. Basic characteristics of niobium and of the niobium–oxygen system

Niobium is a chemical element of group VB of the Periodic System, atomic number 41, atomic mass 92.9064, and electron configuration of the outer electron shell of an Nb atom $4d^4 5s^1$. The main physical properties of metallic niobium are given in Table 1.

Niobium has a body-centered cubic (bcc, space group $Im3m$) lattice in which there exist two types of interstices: octahedral and tetrahedral. The octahedral pores are located in the $(0, 0, 1/2)$ type positions and in those equivalent to them; the tetrahedral pores are in positions of the $(1/2, 0, 1/4)$ type (Fig. 1). The most close-packed structural elements in the bcc structure are planes of the (110) type, and directions of the [111] type (Fig. 1d). These structural features of bcc Nb determine the positions of the localization of the dissolved atoms of metalloids (nitrogen, oxygen, carbon) and the preferable mutual orientation relations with the lattices of phases that are formed in the process of structural and chemical transformations.

Table 1. Physical properties of niobium.

Property	Magnitude
Atomic number	41
Atomic mass, a.m.u.	92.90638
Atomic radius, Å	1.46
Density, g cm^{-3} (293 K)	8.57
Electron configuration	[Kr] $4d^4 5s^1$
Superconducting transition temperature, K	9.25
Melting temperature, K	2741
Boiling temperature, K	5015
Vapor pressure, mmHg	10^{-11} (1953 K); 10^{-5} (2467 K); 10^{-4} (2628 K)
Thermal conductivity, W m^{-1} K^{-1} (273 – 373 K)	54.1
Molar heat capacity, J K^{-1} mol^{-1}	0.268
Specific heat of sublimation, kJ g^{-1} atom^{-1} (298 K)	722.2
Specific heat of boiling, kJ g^{-1} atom^{-1} (t_b)	683.7
Ionization potential, eV	6.77
Work function, eV	4.01
Lattice structure	bcc
Lattice period, Å	3.294
Debye temperature, K	275

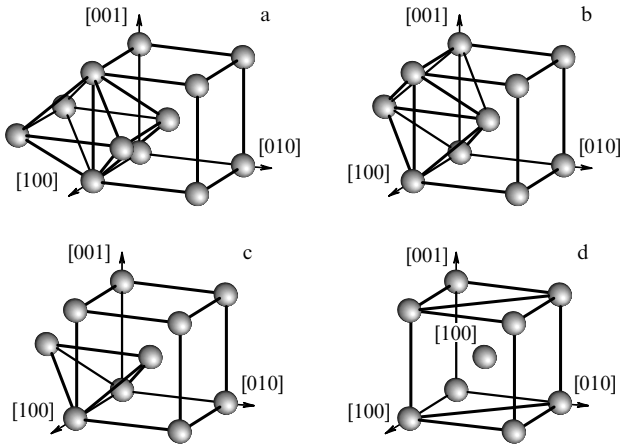

Figure 1. Lattice structure of bcc niobium: (a, b) octahedral interstices; (c) tetrahedral interstice, and (d) the most close-packed Nb(110) plane.

The most common and most important (from the practical viewpoint) structures are the oxide ones that are formed on the Nb surface upon adsorption of oxygen or its segregation from the bulk of the metal.

The character of interactions in the Nb–O system is illustrated by the phase diagram of this binary system (Fig. 2) constructed for a pressure of 133 Pa [13]. Upon interacting with oxygen, niobium forms an α-Nb(O) solid solution with a bcc lattice and three stable oxide phases: NbO, NbO_2, and Nb_2O_5, which exist to temperatures of 2218, 2188, and 1768 K, respectively. The higher oxide Nb_2O_5 has numerous structural modifications; several intermediate oxides with the composition $NbO_{2.42-2.50}$ have also been found. Upon heating in air or in an oxygen atmosphere, all lower oxides are oxidized to Nb_2O_5.

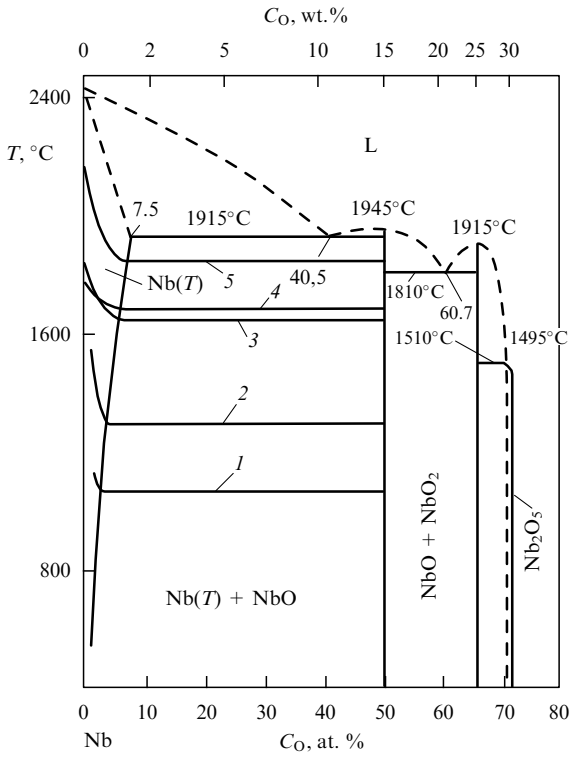

Figure 2. Phase diagram of the Nb–O system [13].

Table 2. Crystal structure and lattice parameters of phases in the Nb–O system [17].

Oxide	Crystal system	Unit cell parameters				Number of formula units per unit cell	Space group
		a, nm	*b*, nm	*c*, nm	Angle, deg		
NbO	Cubic	0.42101	—	—	—	3	$Pm3m$
α-NbO_2	Tetragonal	1.3690	—	0.59871	—	32	$I4_L/a$
β-NbO_2	Tetragonal	0.9693	—	0.59875	—	16	$I4$
β-$Nb_{12}O_{29}$	Orthorhombic	2.072	0.3825	2.899	—	4	$Cmcm$
α-$Nb_{12}O_{29}$	Monoclinic	2.073	0.3835	1.767	112.90	2	$C2/m$
$Nb_{22}O_{54}$	Monoclinic	2.186	0.3822	1.575	122.50	1	—
$Nb_{25}O_{62}$	Monoclinic	2.990	0.3827	2.119	94.97	2	$C2/m$
$Nb_{47}O_{116}$	Monoclinic	5.774	0.3823	2.118	105.32	2	—
α-Nb_2O_5	Orthorhombic	0.623	4.380	0.391	—	12	—
α′-Nb_2O_5	Monoclinic	1.273	0.488	0.556	105.10	4	$C2/m$
β-Nb_2O_5	Monoclinic	2.126	0.3821	1.935	119.74	14	$P2$

The crystallographic data for stable niobium oxides are given in Table 2 and in Fig. 3; their thermodynamic properties are listed in Table 3. Niobium exhibits high oxidation susceptibility; all oxide phases have large values of formation enthalpy and Gibbs energy.

Notice the following substantial structural and chemical properties of phases in the niobium–oxygen system. First, the α-Nb(O) solid solution exists only in a narrow concentration range. This markedly distinguishes niobium from the group IV transition metals (Ti, Zr, and Hf) with a hexagonal close-packed (hcp) lattice. The maximum concentration of dissolved oxygen in the bcc lattice of niobium does not exceed 7.5 at. %. Experiments on proton channeling and measurements of internal friction show that the preferable sites for the incorporation of oxygen atoms into the α-Nb structure are octahedral interstices [14, 15]. All stable niobium oxides have narrow homogeneity ranges. In addition, in the concentration range between the α-Nb(O) and NbO phases there have been revealed a number of metastable lower suboxides NbO_x ($x \sim 1/6, 1/4, 1/2$), which are formed upon the decomposi-

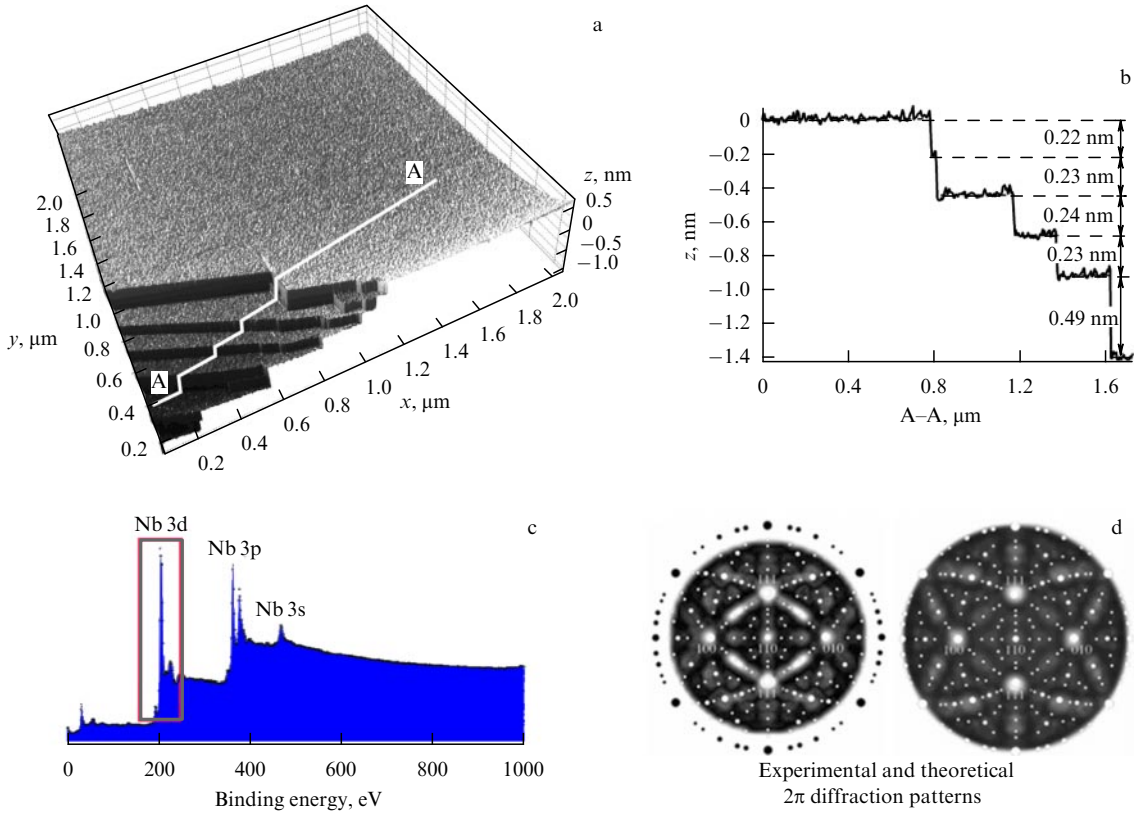

Figure 3. (a) STM image of the Nb(110) surface of single-crystal niobium ($V = 0.1$ V, $I = 2.6$ nA); (b) height profile of the surface; (c) survey XPS spectrum, and (d) XPD patterns of Nb 3d electron scattering (left-hand pattern, experiment; right-hand pattern, single-scattering cluster (SSC) calculations of normal photoelectron diffraction) [19].

Table 3. Physicochemical properties of niobium oxides [18].

	NbO	NbO_2	Nb_2O_5
Melting temperature T_m, °C	1945	1917	
Density ρ, g cm^{-3}	7.26	5.98	
Molar heat capacity C_p^0, J mol^{-1} K^{-1}	41.25	57.49	
Formation enthalpy $-\Delta H_{form}^0$, kJ mol^{-1}	408.2	799.3	1900.8
Molar entropy of evaporation S_{298}^0, J mol^{-1} K^{-1}	—	54.55	137.3
Gibbs energy $-\Delta G_{form}$, kJ mol^{-1}	375.48	741.28	1772.71

tion of supersaturated solid solutions of oxygen in niobium [16]. The suboxide phases are intermediate species corresponding to a gradual transformation of the bcc lattice of α-Nb(O) into the NbO structure. The low solubility of oxygen in the bcc lattice of niobium, the formation of lower suboxide phases already at small concentrations of oxygen, and the high magnitudes of the enthalpy and free energy of formation of oxide phases (see Table 3) indicate the possibility of the formation, along with stable oxide phases, of various intermediate suboxide structures on the faces of single-crystal niobium in a vacuum. Notice that all the above-mentioned phases, including the metastable ones, were revealed when studying the kinetics of niobium oxidation (in the form of foils and bulk samples), with the suboxide structures arising in the form of thin films at the initial stages of Nb oxidation at low oxygen pressures.

For obtaining a pure niobium surface and for studying the adsorption properties of the niobium–oxygen system, information on the kinetic characteristics of the interactions in this system is important. The kinetics of interaction in the niobium–oxygen system at low pressures in the realm of the bulk solid solution is characterized by high values of the adsorption coefficients (r) up to high temperatures (2000–2200 °C); the rate of oxygen adsorption $v = 1.16 \times 10^3 r p_{O_2}$, where p_{O_2} is the oxygen pressure. The processes of oxygen dissolution and diffusion in niobium are not the limiting stages. The competition of the processes of oxygen dissolution in niobium and the removal of oxides begin to show up at temperatures above 1800 °C.

3. A pure niobium surface: experiments and calculations

At present, there exist a very limited number of papers devoted to the experimental investigations of a pure niobium surface. This is explained by substantial technical difficulties in the preparation of such a surface. By a pure surface, we mean, first of all, single-crystal niobium faces free of impurities and possessing a perfect atomic structure. Of certain interest are also surfaces of polycrystalline niobium samples (e.g., films) and niobium-based nanomaterials such as niobium nanoparticles and nanoclusters. The available evidences on the experimental and theoretical studies of a pure niobium surface are collated in Table 4.

In bcc niobium, the most close-packed structure elements are Nb(110), Nb(100), and Nb(111) sectional planes (see Fig. 1). The majority of investigations of pure niobium surfaces and adsorption structures on niobium were performed on these very faces.

The procedures that permit obtaining pure Nb(110) and Nb(100) surfaces were described in detail in Refs [19, 20]. After mechanical and electrochemical polishing of an Nb single-crystal face, the surface is subjected to bombardment by a beam of argon ions and is annealed to approximately 2300 K in an ultrahigh vacuum (UHV) (more than 10^{-8} Pa) by flash heating to remove argon implanted into the surface layers and to form a perfect surface structure. The chemical purity of the surface is controlled by the methods of XPS and Auger electron spectroscopy (AES), while the structural order employs the methods of low-energy electron diffraction (LEED), XPD, or STM.

Figure 3 displays a survey XPS spectrum, XPD patterns of Nb 3d photoemission, and an STM image of a pure Nb(110) surface prepared by the technique described in Ref. [19]. Due to intense diffusion of niobium atoms at high annealing temperatures, a smooth surface consisting of extended Nb(110) terraces separated by monolayer (ML) steps with faceted boundaries is formed. The crystal surface obtained can be considered smooth, since the total difference in height in a region with an area of $\sim 2\ \mu m^2$ is only 1.65 nm, and the steps correspond to one or two monolayers of the Nb(110) face. The average height of a step measures 2.3 Å, which is close to the interplanar spacing in the bulk bcc niobium in the [110] direction ($d = 2.33$ Å). The XPD data (Fig. 3d) confirm the correspondence of the surface obtained to the (110) plane of bcc niobium, and the XPS data indicate the oxygen content on the surface at a level of a few percent. Unfortunately, even under UHV conditions ($\sim 10^{-8}$ Pa) such a surface is retained only for a short time (several dozen hours) and is gradually covered by oxide (apparently, amorphous) structures.

An important issue in the characterization of the prepared surfaces of an Nb single crystal is the investigation of the effects of structural relaxation of surface layers, which can lead to a noticeable change in the interplanar spacings near the surface.

Experimentally, these effects can be studied invoking XPS. The authors of Ref. [21] obtained XPS spectra of inner Nb $3d_{5/2}$ states from a single-crystal Nb(001) face using synchrotron radiation (Fig. 4a). To enhance the sensitivity, X-ray quanta with energies $h\nu = 240$ and 250 eV were utilized; in this case, the kinetic energy of Nb 3d electrons is only several dozen electron-volts and the probing depth does not exceed two–four surface monolayers. The magnitude of the chemical shift of the Nb $3d_{5/2}$ levels of niobium surface states relative to the spectral line emitted from the bulk of the metal (the so-called surface core-level shift, SCLS) for the outermost monolayer was $S_1 = 0.49 \pm 0.01$ eV [21] in the direction of greater binding energies E_b counted from the ground state; for the second monolayer, the appropriate shift is $S_2 = 0.13 \pm 0.01$ eV, being also taken in the direction of greater E_b, which agrees well with the results of *ab initio* calculations [22].

The surface states of Nb(001) in the valence band have been studied [23] using ultraviolet (UV) spectroscopy and photoemission initiated by synchrotron radiation. In the UV spectra, the surface states (resonances) lie in the immediate vicinity of the Fermi level (E_F); their binding energy is as small as $E_b = -0.06$ eV. In Fig. 4b, the surface states are designated as S; the bulk 4d states of Nb are designated as B. In the case of the UV spectra of the valence band of Nb(110), an intense maximum due to Nb 4d states from the bulk of the

Table 4. Studies of the pure niobium surface and of adsorption and oxide structures on the surface of polycrystalline and single-crystal niobium.

System	Research methods *	References
Nb(110)	XPS, XPD	[52]
	VASP calculations	[32]
	NRL-TB calculations	[31]
	FP-LMTO calculations	[30]
O/Nb(110)	AES, LEED, TDS, CPD	[38, 53]
	LEED, HREELS	[35]
	STM, AES, XPS	[45]
	LEED, XPS, XPD	[51]
	STM, XPS, AES, LEED	[47, 49, 50]
	AES, RHEED, STM, STS	[46]
	AES, LEED, WF	[41]
	XPS, XPD	[27, 54, 55]
	XPS, UVS, AES	[56]
Y_2O_3/NbO/Nb(110)	LEED, XPS, XPD	[57]
C, O, H_2O, CH_3OH/Nb(110)	HREELS, AES, UVS	[24, 58, 59]
	HREELS, AES, LEED	[60]
	CASTEP calculations	[61]
N_2/Nb(110)	UVS	[62, 63]
	UVS, electric conductivity	[64, 65]
H_2/Nb(110)	Theoretical simulation	[66, 67]
Nb(100)	XPS, synchrotron radiation	[21]
	XPS, synchrotron radiation	[23]
	XPS, synchrotron radiation	[68, 69]
	NRL-TB calculations	[31]
	FP-LMTO	[30]
	XPD	[70]
O/Nb(100)	AES, LEED, STM	[20, 41, 48, 71]
	XPS, synchrotron radiation	[72]
	Energy-band calculations	[28, 29]
	AES, LEED, TDS, CPD	[37]
S/Nb(100)	XPS	[73]
	STM, AES, LEED	[74]
N/Nb(100)	LEED, AES	[75, 76]
N/Nb(100)	XPS, synchrotron radiation	[77]
	HREELS	[78]
H/Nb(100)	STM	[79]
	Molecular dynamics calculations	[80]
Nb(111)	Photoemission spectroscopy	[81]
	NRL-TB calculations	[31]
O/Nb(111)	AES, LEED, TDS, CPD	[39, 41]
Nb (polycryst.)	ARXPS	[82]
Nb (nanocluster)	TBMD calculations	[83]

Table 4 (continued)

System	Research methods *	References
O/Nb	XPS	[84]
$H/NbO_x/Nb$	AES, TDS	[85]
Nb_2O_5/Nb	XPS	[86]

* AES, Auger electron spectroscopy; LEED, low-energy electron diffraction; STM, scanning tunneling microscopy; TDS, thermal desorption spectroscopy; CPD, contact potential difference; HREELS, high-resolution electron energy loss spectroscopy; XPS, X-ray photoelectron spectroscopy; ARXPS, angle-resolved X-ray photoelectron spectroscopy; UVS, ultraviolet spectroscopy; XPD, X-ray photoelectron diffraction; RHEED, reflection high-energy electron diffraction; STS, scanning tunneling spectroscopy; WF, work function; FP-LMTO, full-potential linear muffin-tin orbital method; NRL-TB, Naval Research Laboratory tight binding method.

crystal was observed, located 0.4 eV below E_F; no surface states were resolved.

To determine the magnitude of the interlayer contraction for two upper layers of the Nb(100) surface, an interesting XPD experiment was performed in Ref. [25]. Intensities of photoemission of Nb 3d electrons were measured depending on the polar angle θ for several azimuthal directions (at angle ϕ) on the Nb(100) surface. The energy $h\nu$ of incident quanta amounted to 1253.6 eV (Mg K_α radiation); at $E_b(\text{Nb } 3d_{5/2}) \sim$ 202.3 eV, the kinetic energy of the photoelectrons is $E_{kin} \sim 1050$ eV. At these high energies, the model of the direct scattering of photoelectrons by atoms of the nearest environments is realized, in which the geometry of the nearest environment of niobium atoms can be estimated from the maxima in the $I(\theta)$ angular dependences. In addition, in Ref. [25] calculations were performed of the angular dependences of XPD in the approximation of multiple scattering of photoelectrons (MSC-SW), and a model of an Nb(100) surface was suggested which agrees quite well with experiment. The so-called Pendry R factor was implicated [26], which determines the average value of the discrepancy between the experimental and theoretical XPD curves. It turned out that the minimum value of R is achieved upon a contraction of the upper Nb(100) layers by 12.7% relative to the interplanar spacing in the bulk of the Nb crystal.

Analogous XPD experiments for the Nb(110) face were performed in Refs [19, 27]. Figure 3d displays the total 2π diffraction pattern of Nb $3d_{5/2}$ photoelectrons ($E_{kin} = 1050$ eV). It can be seen that the distribution of the main diffraction maxima of the (110) face exhibits a characteristic twofold symmetry and agrees well with the stereographic projection for the cubic structure with the orientation along the [110] direction. The XPD calculations in the approximations of single (SSC) and multiple (MSC)

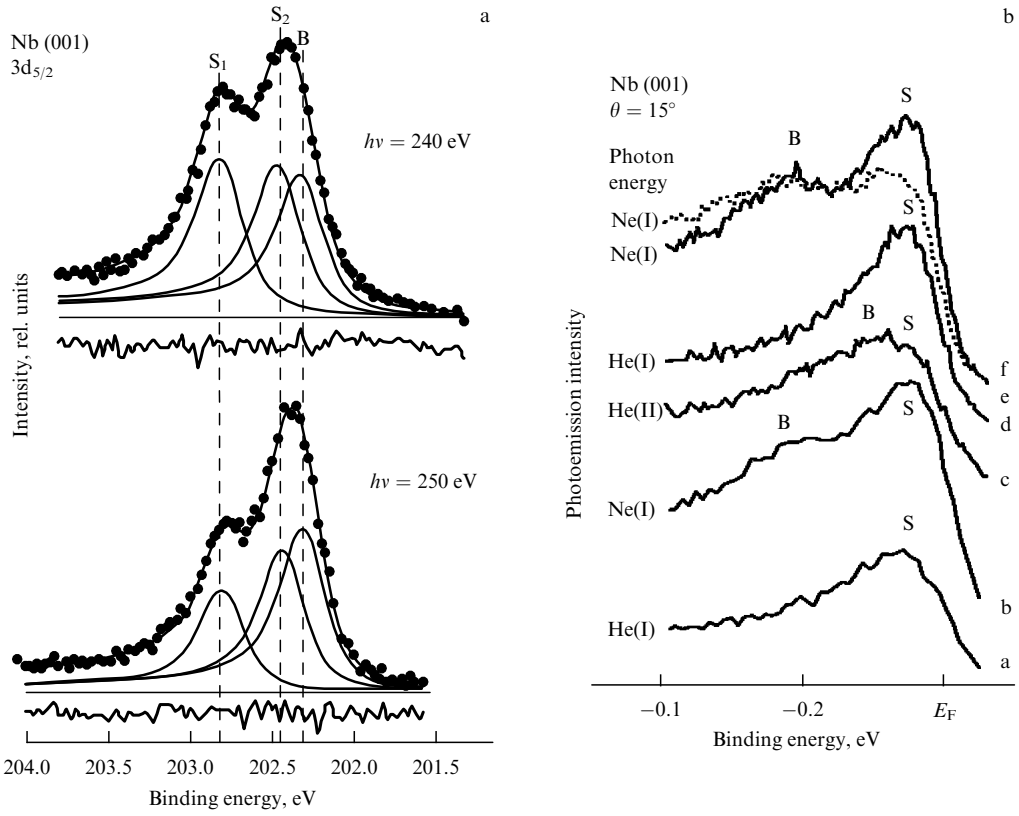

Figure 4. (a) Photoelectron Nb $3d_{5/2}$ spectra of the Nb(001) surface at $T = 130$ K recorded at the incident photon energies 240 and 250 eV [21]. States from the bulk of the Nb(001) crystal (B), and from the first and second surface monolayers (S_1 and S_2, respectively) are indicated. (b) Ultraviolet spectra of the Nb(001) surface [23] for different sources of photons: B, bulk Nb 4d states; S, surface resonance states.

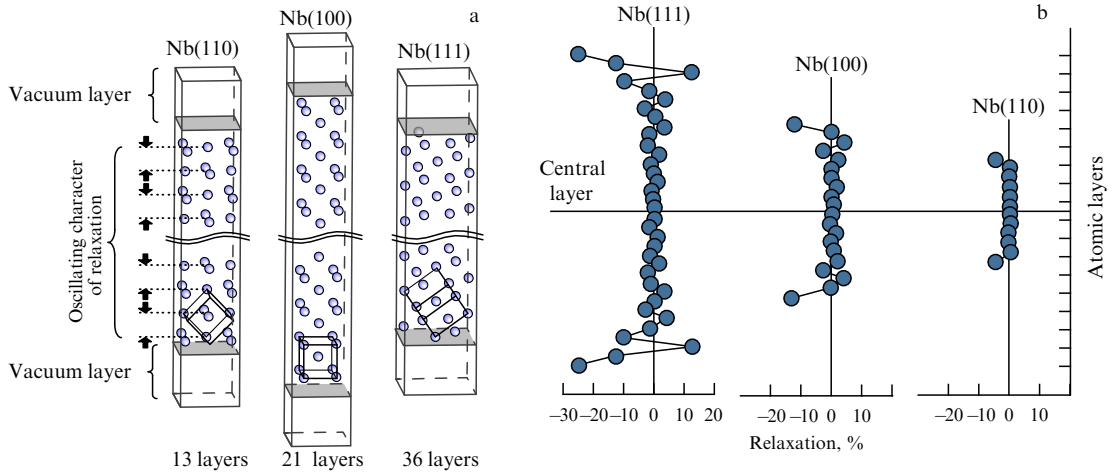

Figure 5. (a) Supercells used for simulating Nb(110), Nb(100) [32], and Nb(111) [31] faces. The arrows indicate the directions of the displacements of Nb monolayers. (b) Change in the interlayer spacing (in percent, relative to the bulk of the Nb crystal) for the Nb(100) [32], Nb(110) [32], and Nb(111) [31] faces.

scattering of electrons showed that the contraction of the upper layers of the Nb(110) face relative to the interlayer spacing in the bulk of the Nb crystal does not exceed 5%.

The technical difficulties in the preparation of atomically pure niobium surfaces and in the experimentation under UHV conditions ($< 10^{-8}$ Pa) render experiments on the computer simulation of the properties of Nb surfaces by modern *ab initio* quantum-theoretical methods topical.

In these calculations, quasi-two-dimensional supercells (slabs) are usually employed for the simulation of surface states of metals (including Nb), which consist of a set of atomic monolayers (MLs) of Nb separated by several 'empty' layers imitating vacuum (Fig. 5a). The central part of the supercell corresponds to the bulk of the metal, and the two outer layers correspond to its surface. In the starting geometry, the interlayer spacings are equal, which is characteristic of the bulk of the metal, e.g., bcc Nb. In the process of approaching self-consistency, the atomic positions become optimized, permitting one to determine the surface relaxation effects. For example, the self-consistent structure of an Nb slab represents an 'accordion' structure in which the interlayer spacings deviate from the initial value; these deviations are shown (in percent) in Fig. 5b.

The authors of Refs [28, 29] performed an analysis of the main features of the dispersion of the energy bands in surface monolayers near the Fermi level for the Nb(100) face in terms of the self-consistent pseudopotential method. The estimates of the surface energy E_{surf} with allowance for relaxation effects indicated that the (100) surface, relative to the (110) and (111) ones, has a minimum value of E_{surf} and that for all the faces (100), (110), and (111) a contraction of subsurface layers is observed. Close results were obtained by applying the tight-binding (TB) method and the full-potential linear muffin-tin orbital (FP-LMTO) method [30].

The authors of paper [31] used the TB method in the NRL-TB parametrization for the investigation of the main Nb faces (100), (110), and (111) and established that the contractions for the two uppermost layers were: 11.7% for Nb(100), 5.8% for Nb(110), and 24.8% for Nb(111). Analogous calculations by the projector augmented-wave method (VASP-PAW package) were performed in work [32] for the Nb(100) and Nb(110) surfaces. According to the data obtained, the relaxation contraction for the (100) and (110) faces was 13.1 and 4.3%, respectively.

It follows from the calculations that the relaxation distortions on the close-packed (110) surface prove to be many fewer than for the 'looser' (100) surface and, all the more so, for the Nb(111) surface. In the case of Nb(110), the first two layers are contracted by only 4.3% (relative to the 'bulk') and the total relaxation involves no more than two–three surface monolayers. On the Nb(111) surface, the relaxation involves almost ten surface layers and exhibits a decaying harmonic character. The two uppermost monolayers contract by $\sim 25\%$; the following layers also contract, by 12%; next, there is an increase in the interlayer spacing by $\sim 12\%$; then, again contraction, expansion, etc. take place, with the amplitudes of the relaxation gradually decreasing when moving away from the surface. Therefore, if the Nb(111) film has a thickness of less than 20 monolayers, all its layers will take part in the relaxation. As a result, the properties of such ultrathin films will differ markedly from the properties of a 'bulk' niobium crystal. The calculations also predict that the properties of ultrathin Nb films with different orientations [e.g., (110), (100), (111)] should also be substantially different because of the differences in the interlayer spacings and, as a consequence, because of the differences in the electronic structure of such films.

4. Adsorption structures on the niobium surface

To date, vast experience has been accumulated on the creation and investigation of adsorption structures, nanolayers, and thin films of nitrides, carbides, and oxides on the surfaces of transition d-metals; part of these findings was presented in the monograph [33]. In this section, we mainly focus on the niobium–oxygen system, while also considering the most interesting examples of the investigation of gas adsorption on some other d-metals of groups IV–VI of the Periodic System.

4.1 Adsorption properties of d-metal–oxygen systems: early studies

Among the earlier work, of most interest is the review [34] which generalizes the experimental data on the interaction of

Table 5. Some parameters of the process of oxygen (O_2) adsorption on films of transition d-metals: ratio of the heat of oxygen solution in the metal (ΔH_s) to the activation energy for bulk diffusion (A_D), and maximum amount of adsorbed nitrogen in various states (the roughness factor of a film surface was equal to 2–3) [34].

Metal	$\Delta H_s/A_D$	Physical adsorption		Molecular chemisorption		Chemisorption + adsorption layer	
		$N \times 10^{-13}$, molecules cm^{-2}	T, K	$N \times 10^{-14}$, molecules cm^{-2}	T, K	$N \times 10^{-15}$, molecules cm^{-2}	T, K
Ti, Zr, Hf	−2.6	—	—	1–2	77	6–16	< 360
V, Nb, Ta	−3.5	—	—	2–4	77	8–12	< 360
Mo, W	−2.4	—	—	5–6	77	6–9	< 360
Re, Fe, Ni	−1.6	—	—	8–9	77	7–9	< 360
Cu, Ag	−0.5 + 1	—	—	—	77	0.6–1.2	< 330

oxygen with transition-metal films. The authors of the review suggested an interpretation of the adsorption properties of metals proceeding from the physical characteristics of bulk metals, such as the heat of an oxygen solution in a metal, ΔH_s, and the activation energies for bulk diffusion of oxygen, A_D. To determine the energy–reaction path diagram for the gas molecules on the metal surface, we should additionally know the heats of molecular adsorption (physical adsorption or molecular chemisorption) ΔH_p, dissociative chemisorption ΔH_c, and segregation ΔH_{seg}, as well as the activation energies for the surface dissociation of gas molecules, A_d, and for the penetration of adatoms under the surface, A_s.

Examples of typical energy–reaction path diagrams [34] are given in Fig. 6, where the first curve (a) characterizes physically adsorbed systems or systems with molecular chemisorption; here, the quantities ΔH_s and A_D are positive and sufficiently large and at relatively low temperatures only physical adsorption is possible. In diagrams (b) and (c), ΔH_s is also positive (endothermic system), whereas the heat of chemisorption ΔH_c (*3*) is negative. Under these conditions, a dissociative chemisorption of oxygen with a coverage $\vartheta < 1$ is possible and thermal activation is required because of the existence of a high activation barrier A_d. In metal–oxygen systems with an exothermic dissolution reaction, the formation of an adsorption layer is also possible, i.e., the penetration of oxygen into the surface layers can occur through both low-energy adsorption centers and defects in the structure of the thermodynamically stable sorption layer (shown by dashed lines in Figs 6d, 6e). In those systems where the heat of chemisorption ΔH_c is less than the heat of solution ΔH_s (diagrams in Fig. 6d), a noticeable surface segregation is observed, i.e., an accumulation of adsorbate atoms on the surface and in the subsurface layers of the metal. The penetration of oxygen into deeper layers is possible if it overcomes the activation barrier A_D for bulk diffusion.

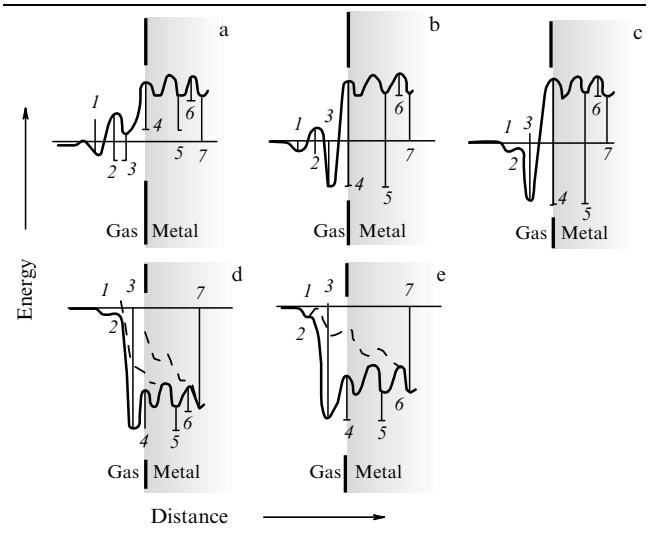

Figure 6. (a–e) Possible variants of the interaction potentials of O_2 molecules with the surface of a d-metal [34]: (*1*) ΔH_p is the heat of molecular adsorption; (*2*) A_d is the activation energy for the dissociation of gas molecules on the surface; (*3*) ΔH_c is the heat of dissociative chemisorption; (*4*) A_s is the activation energy for the penetration of adatoms under the surface; (*5*) ΔH_{seg} is the heat of segregation of adatoms under the surface; (*6*) A_D is the activation energy for oxygen bulk diffusion, and (*7*) ΔH_s is the heat of oxygen solution in the metal.

As is seen from Table 5, the group V metals, including niobium, are characterized by the formation of an adsorption layer at room temperature and of chemisorbed molecular (or atomic) states. At $T \sim 77$ K, only molecular chemisorption of gases occurs on the surface.

Later investigations of some d-metals refined this picture and, in the case of niobium, disproved the conclusions drawn in Ref. [34]. Thus, a detailed investigation [35] of oxygen adsorption on an Nb(110) single-crystal face, performed using spectral (HREELS, AES) and diffraction (LEED) methods at room temperature ($T = 300$ K) and lower (80 and 20 K), showed that at 300 and 80 K the oxygen adsorption (0–32 L)[1] is accompanied by a dissociative decomposition of oxygen molecules (O_2), a chemisorption of arising atomic oxygen, and a growth in oxide layers $NbO + NbO_2$. On the surface of NbO and NbO_2 layers, traces of Nb_2O_5 molecules were also revealed. At $T \sim 20$ K, a layer of physically adsorbed molecular oxygen is additionally formed on the surface of the oxides.

It should be noted that the investigations in Ref. [34] were performed on polycrystalline samples, which is important for solving some practical problems. On the other hand, for a detailed description of the mechanism and kinetics of adsorption on an atomic (molecular) level studies are required on the surfaces of single-crystal faces.

A large cycle of such studies on the oxygen adsorption on single-crystal faces of niobium and tantalum was performed by the authors of Refs [36–40]. The kinetics of oxygen adsorption on the surface of niobium (tantalum) and the surface structural transformations at various coverages of the metals by oxygen were studied using the AES, LEED, thermal desorption spectroscopy (TDS), and contact potential difference (CPD) methods. After oxygen sedimentation at room temperature, the crystals were annealed at temperatures of up to $T = 1600$ K, and the thermal stability of adsorption

[1] 1 L (1 langmuir) corresponds to the sample exposure at a gas pressure of 1.33×10^{-4} Pa for 1 s.

structures formed at the surface and the scales of oxygen diffusion into the bulk of the metal were studied. It has been established that upon oxygen adsorption in a vacuum at $T = 300$ K, no dissolution of oxygen in Nb and Ta occurs; a niobium (tantalum) monoxide is formed on the surface of a metal or, to be precise, a facet cut of the corresponding oxide whose structure and thickness depend on the metal single-crystal surface chosen, temperature, and oxygen concentration on the surface. For example, for the most close-packed Nb(110) facet, a single NbO monolayer (maximum value of coverage $\vartheta_{max} \sim 1$) is formed on its surface; on the Nb(100) facet, the thickness of the oxide is equal to 2 ML ($\vartheta_{max} \sim 2$), and for the most 'open' Nb(111) facet it is 3 ML ($\vartheta_{max} \sim 3$). The oxygen adsorption on the Nb(110) and Nb(100) surfaces is accompanied by the formation of a number of different surface structures, depending on the oxygen content on the surface; in the case of the Nb(111) facet, no ordered structures formed on the surface. The set of phase states and the specific features of the kinetics of oxygen sorption on the Ta(110) facet on the whole replicates those observed for the Nb(110) facet [36–40].

The vacuum annealing of oxide structures on Nb and Ta surfaces leads [38, 40] to the consecutive destruction of surface oxide phases and to oxygen dissolution in the bulk of niobium and tantalum, with the processes observed differing significantly for different crystal faces. For example, for close-packed (110) faces of Nb and Ta, the phase states of the surface layer change reversibly with a variation in the oxygen concentration both due to adsorption and upon vacuum annealing. On the contrary, no such reversibility is observed on the Nb(100) and Nb(111) faces; this can be related to specific features of the rearrangement of these faces, which involves several atomic layers of metal, when three-dimensional structures of a bulk oxide are formed that cannot develop further under the conditions of an oxygen deficit on the surface.

The assumption [36] about the oxygen dissolution going from the surface oxides into the bulk of niobium upon annealing in a UHV is interesting, but it requires refinement. According to later evidence [20], amorphous oxides are formed on the niobium surface at room temperature in the following sequence: $NbO \rightarrow NbO_2 \rightarrow Nb_2O_5$ due to the presence of residual gases or oxygen (O_2) adsorption. Upon annealing in a UHV at $T = 598$ K, the pentoxide Nb_2O_5 is reduced to the dioxide NbO_2 and further to monoxide NbO owing to the oxygen dissolution in the bulk of the metal; at a temperature of 227 K, the monoxide begins evaporating.

4.2 Oxygen-induced adsorption structures on Nb(110) and Nb(100) faces

Of all the oxides that are formed on the niobium surface, of most interest are those with a small content of oxygen, i.e., monoxide and suboxides NbO_x ($x \leqslant 1$). The progress that was achieved in the investigation of the structure and properties of surface layers of this type in the last several years is mainly due to the use of a combination of spectral, diffraction, and microscopic methods of studying the surface, as well as due to the development of reliable methods of preparation of an ultrapure niobium surface. Table 4 collates the available experimental and theoretical data on the adsorption and oxide structures formed on the surfaces of polycrystalline and single-crystal niobium samples.

The morphology of oxygen-induced structures on the Nb(100), Nb(110), and Nb(111) surfaces was studied in much detail by the LEED method. A faceted structure [41, 42], O (3×1) [42, 43], O (4×1) [43], and O $c(2 \times 2)$ [41–43] structures, and a pure (1×1) Nb(100) structure [41–44] were observed on the Nb(100) surface in the process of its annealing under UHV conditions in a temperature range of 1973–2673 K. After the preparation of a pure Nb(100) surface, oxygen was adsorbed on it at room temperature, and the formation of an O $c(2 \times 2)$ structure and the diffusion O (1×1) structure was observed [41]. The O (3×1) and O (4×1) structures revealed with the LEED method were assigned to oxide (NbO and NbO_2) structures using photoelectron spectroscopy [43], whereas O $c(2 \times 2)$ and O (1×1) structures formed due to the chemisorbed oxygen [41]. The exact spatial geometry of atoms in these oxygen-induced structures has not yet been established.

The oxide structures on the surfaces of Nb(100) [45] and Nb(110) [46, 47] single crystals have been studied by STM. In particular, the pyramidal protrusions [45] on Nb(100) surface (cleaned by Ar^+ ion bombardment and annealed to $T = 1273$ K) were interpreted as isolated NbO nanocrystals grown epitaxially on the Nb(100) surface. In Ref. [48], ladderlike superstructures were observed on the Nb(100) surface after cleaning by Ar^+ ion bombardment and flash annealing to 1973 K under UHV conditions. In these experiments, the oxide structures were formed on Nb(100) without the creation of the initially pure (1×1) metal surface; therefore, the evolution of the atomic environment of niobium on the surface and the epitaxial relationships between the lattices of the oxide and the substrate have not been studied.

In Refs [47, 49, 50], thin oxide layers on the Nb(110) surface, which appear as a result of segregation of oxygen dissolved in the niobium bulk after heating in UHV to $T = 1200$–2200 K, have been studied by XPS using synchrotron radiation and by STM. An analysis of the XPS spectra of Nb 3d states made it possible to draw an inference about the complex nature of these layers containing a whole number of niobium oxides (Fig. 7). The two main forms of NbO_x found in this system are (1) $NbO_{0.8} - NbO_{1.2}$ (oxides located on the surface), and (2) $Nb_{1.5}O$ (niobium atoms located in the region of the oxide-layer–metal interface).

Notice that the chemical shift of the maximum B (pertaining to the surface oxide) relative to the band A (metallic niobium) amounts approximately to 1.4 eV (Fig. 7a), which is less than the chemical shift for NbO (1.8 eV) [47]. The STM patterns (Fig. 7c) demonstrate ordered close-packed atomic rows on the niobium surface. It was concluded in Ref. [47] that the surface layer consists of separate linearly ordered $NbO_{x\sim1}$ nanocrystals and contains numerous defects, which accompany the formation of these nanocrystals on the Nb(110) face. The hexagonal close-packed plane (111) of nanocrystals is parallel to the close-packed plane (110) of the niobium substrate, while the $\langle 110 \rangle$ direction of the fcc lattice of the monoxide is parallel to the $\langle 111 \rangle$ direction of the bcc lattice of the metal. The matching between these lattices obeys the Kurdjumov–Sachs orientation relationship (OR).

A different view on the nature of oxide structures formed on the Nb(110) surface was suggested by the authors of Ref. [46], who studied the Nb (110) surface before and after thermal annealing in a vacuum ($T = 1300$ K) by the methods of Auger electron spectroscopy (AES), reflection high-energy electron diffraction (RHEED), STM, and scanning tunneling spectroscopy (STS). STM patterns of the surface analogous

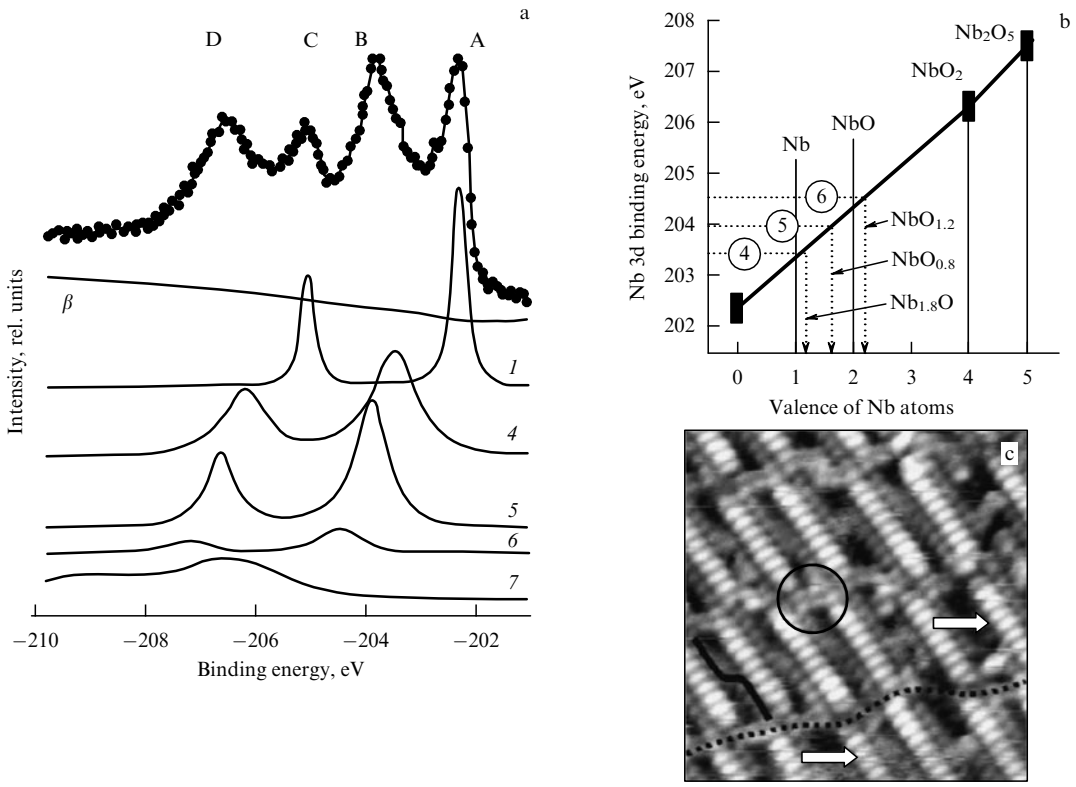

Figure 7. (a) Resolution of the Nb 3d XPS spectrum into components [47] associated with (*1*) metallic Nb(110) substrate, (*4–6*) surface oxide in different forms, and (*7*) pentoxide. (b) Comparison of the results of the resolution with the data on the chemical shift of the Nb 3d line in bulk oxides. (c) Surface oxide ordered structures on the Nb(110) surface [39].

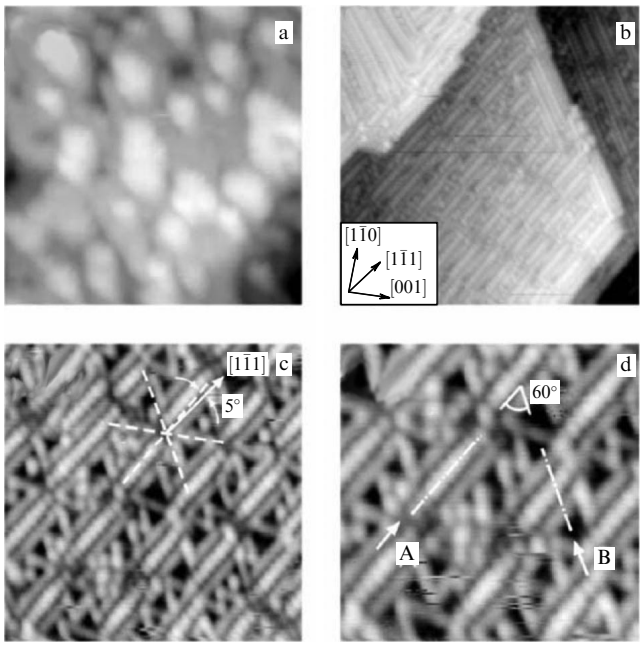

Figure 8. STM images of the Nb(110) surface after (a) cleaning by ionic bombardment in a vacuum, and (b–d) annealing at 1300 K [46].

to those given in Ref. [47] have been obtained; the RHEED experiments revealed the formation of a long-period superstructure turned by 5° relative to the Nb⟨111⟩ direction. By comparing the STM and electron diffraction data, it was concluded [46] that the superstructure formed on the surface is related to the rows of Nb atoms regularly arranged on the surface (Fig. 8). The mutual orientation of the two-dimensional periodic superstructure and the Nb(110) plane, and the relationship between their parameters and interatomic distances indicate that the superstructures arise as a result of accommodation of stresses upon the matching of the Nb(110) surface and growing NbO(111) type layer with the ORs close to NbO[10$\bar{1}$] ∥ Nb[001] and NbO[1$\bar{2}$1] ∥ Nb[1$\bar{1}$0]. The formation of an almost stoichiometric monoxide $NbO_{x\sim1}$ is impeded because this oxide possesses a very narrow homogeneity region and even small deviations from the stoichiometric composition (Nb/O = 1) make the material multiphase. This can be the cause of the local formation of NbO-like regions, in addition to vacancies and other defects. Thus, the authors of Ref. [46] consider the surface structures as oxygen-induced surface layers that serve as precursors for the growth of a niobium monoxide layer rather than as NbO nanocrystals.

STM images excellently demonstrate the morphology of the quasiordered NbO structures mainly due to the electron tunneling from the niobium atoms. In this case, however, the oxygen atoms, both in the surface-sorbed state and in the composition of surface oxide structures, are excluded from the consideration. Information about the localization and chemical state of oxygen atoms on the niobium surface can be obtained from XPS data and from the diffraction patterns of scattering of O 1s and Nb 3d photoelectrons by atoms from the nearest surroundings of niobium atoms.

Appropriate XPD experiments on the diffraction of Nb 3d electrons with the separation of chemical states from the Nb(110) substrate and NbO_x layer permitted the authors of

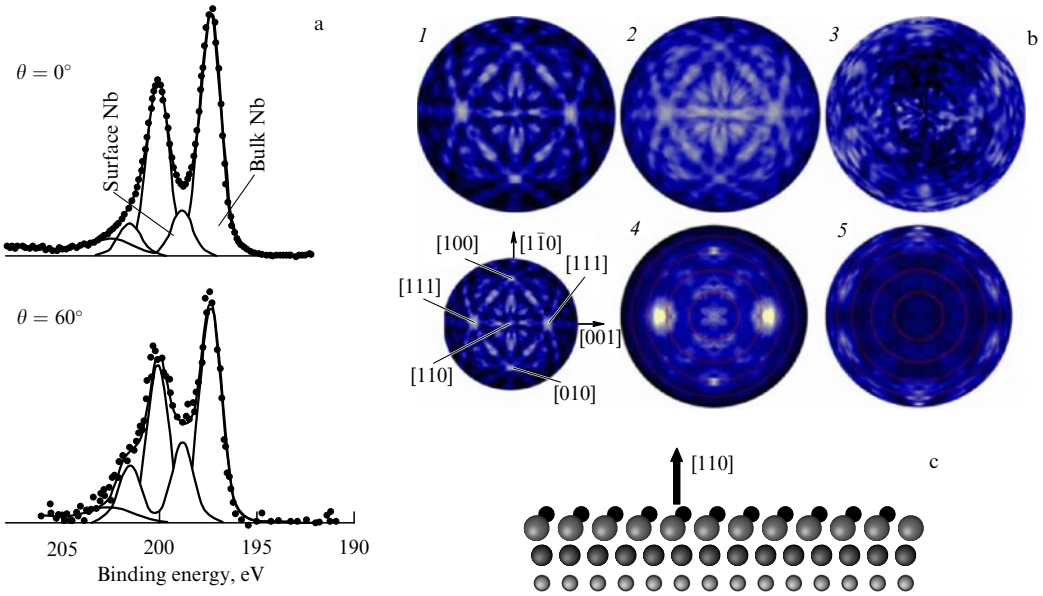

Figure 9. (a)Nb 3d XPS spectra of the NbO/Nb(110) surface, taken in the direction of the normal to the surface and at an angle of 60° off the normal. States relevant to the Nb(110) substrate and the surface NbO layer are singled out. (b) XPD patterns of Nb 3d states: (*1*) total Nb 3d diffraction pattern, XPD patterns of the Nb(110) substrate (*2*) and the surface NbO layer (*3*); and calculated XPD patterns for the Nb(110) substrate (*4*) and the NbO monolayer (*5*). (c) Model of the NbO_x/Nb(110) surface [51].

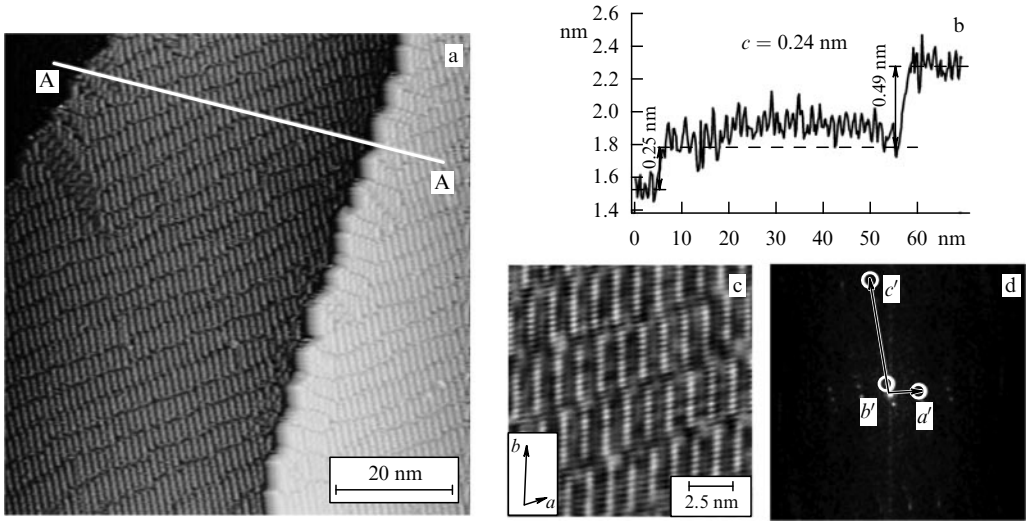

Figure 10. (a, c) STM images of the NbO/Nb(110) surface, (b) height profile of the surface along the A–A direction, and (d) Fourier image of periodic NbO structures on the Nb(110) surface.

Ref. [51] to resolve in the spectrum a surface component shifted relative to the metallic state by 1.6 eV, which was ascribed to the NbO form (Fig. 9a). The thickness of the NbO_x surface layer was estimated to be equal to 4.5 Å, which corresponds to one or two atomic monolayers. The Nb 3d spectra were collected along 4945 different directions over the surface of the sample and resolved into bulk and surface components. For each component, 2π patterns of photoelectron diffraction reflecting the local structure of niobium atoms inside the Nb(110) substrate and the NbO_x layer were constructed (Fig. 9b). An analysis of the diffraction pattern of the oxide component made it possible to establish that the oxygen atoms are localized at a height of approximately 1.2 Å above the niobium surface.

The oxide structures on the Nb(110) surface have been studied in detail by XPS, XPD, and STM [19, 27, 52, 54, 55]. It has been found that the NbO/Nb(110) surface consists of terraces 40–60 nm wide, on which the quasiperiodic structures of niobium oxide are formed (Fig. 10). The height of the steps between the terraces reaches ~ 2.5 and ~ 4.9 Å, which are multiples of the interlayer spacings (1 and 2 ML) in the NbO fcc lattice. The oxide structures are visualized by the STM method as linear chains of 10 ± 1 niobium atoms that are elevated above the surface at the height $d \sim 1.2$ Å. The two possible orientations of the rows of Nb atoms in the ⟨111⟩ directions on the Nb(110) surface are equally probable. As a result, domains are formed in which the linear NbO structures are rotated relative to each other by approximately 60°. The

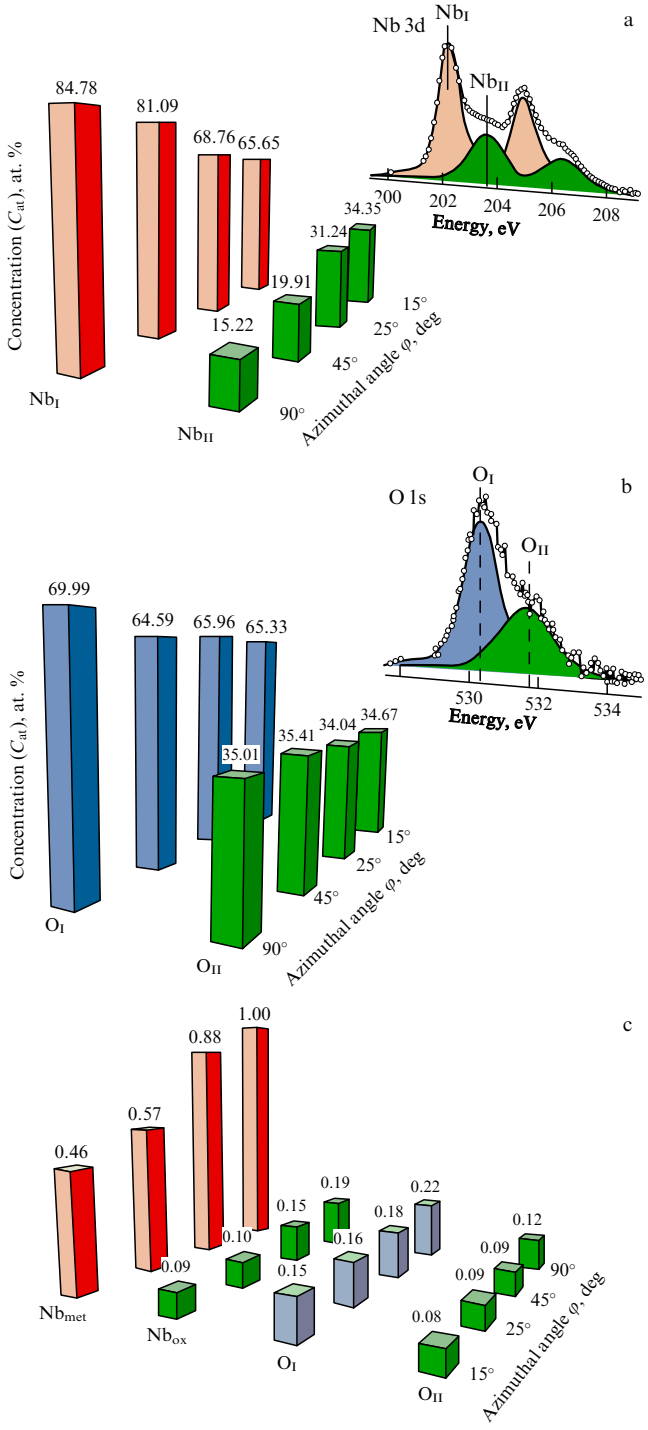

Figure 11. Angular dependences of the Nb 3d (a) and the O 1s (b) spectra taken from the NbO/Nb(110) surface. Contributions of resolved bands in the niobium and oxygen spectra are shown for different angles. (c) Relative concentrations of niobium and oxygen atoms on the surface. The first column corresponds to niobium atoms of the Nb(110) substrate, the second to niobium in the composition of the surface oxide, and the third and fourth to two oxygen forms on the Nb(110) surface: O_{II} is oxygen sorbed on the surface, and O_I is oxygen in the NbO structure [19].

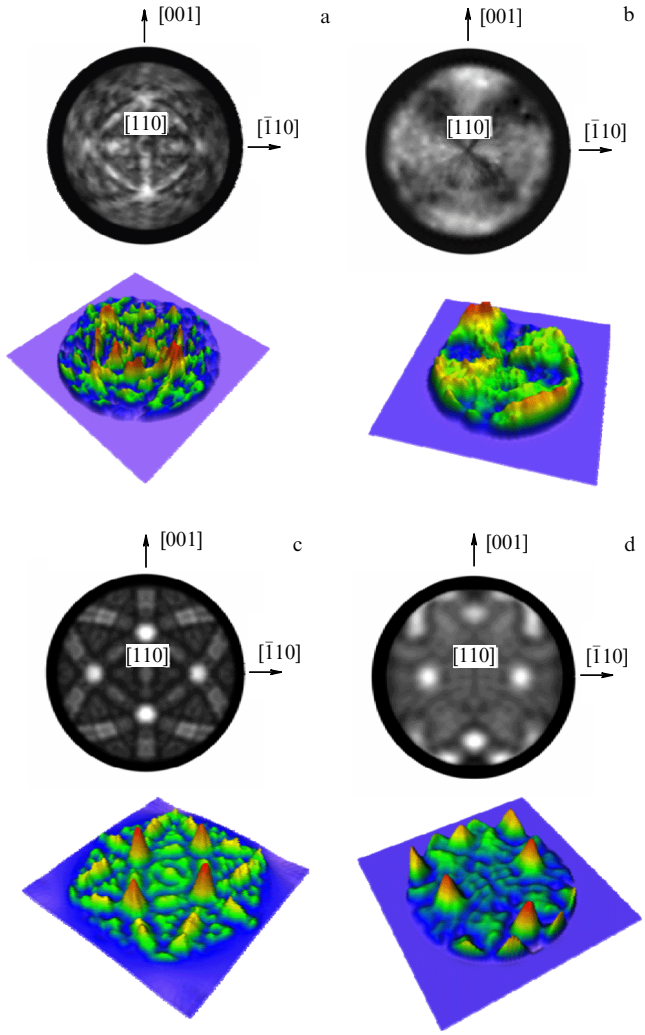

Figure 12. Experimental XPD study and SSC-SW calculations of the NbO/Nb(110) surface: (a, b) experimental diffraction patterns of photoemission for (a) Nb 3d (E_{kin} = 1050 eV) and (b) O 1s (E_{kin} = 720 eV) (upper pictures comply with 2π projections, and the lower ones with three-dimensional images of the XPD patterns); (c, d) SSC-SW calculations of the O/Nb(110) surface: (c) diffraction patterns of the Nb 3d photoemission, and (d) total O 1s photoemission.

Fourier analysis of surface structures revealed plane symmetry groups $p1$ and $p2$; the parameters of the structure periodicity along the a and b directions were determined to be 12.7 and 34.7 Å, respectively.

In the Nb 3d photoelectron spectra of the NbO/Nb(110) surface, two components were distinguished [55], which are related to the Nb atoms of the Nb(110) substrate and surface oxide structures (Fig. 11a). The chemical shift of the Nb 3d band caused by the surface structures relative to that observed in the metal is about 1.56 eV, which is less than the chemical shift for the well-characterized $NbO_{\sim 1.0}$ monoxide (2.25 eV). However, the surface structures possess a number of characteristics inherent in a hypothetical hexagonal layer of the NbO oxide, e.g., the orientation of surface clusters corresponds to NbO(111), and the rows of Nb atoms are deflected through about 5° relative to the Nb⟨111⟩ direction, which coincides with the NbO⟨110⟩ direction [46].

In the O 1s spectra for the NbO/Nb(110) surface, two chemically nonequivalent states were also revealed [19, 55]: at 530.5 eV (O_I), and at 531.85 eV (O_{II}) (Fig. 11b). It has been shown that the band at 531.85 eV corresponds to the chemical form O_{II} in the composition of NbO structures on Nb(110), and the maximum at 530.5 eV is related to the chemisorbed oxygen states on the surface. The ratio between concentrations of these oxygen forms is $O_I : O_{II} \sim 2:1$. By separating the bands corresponding to the surface oxide in the O 1s

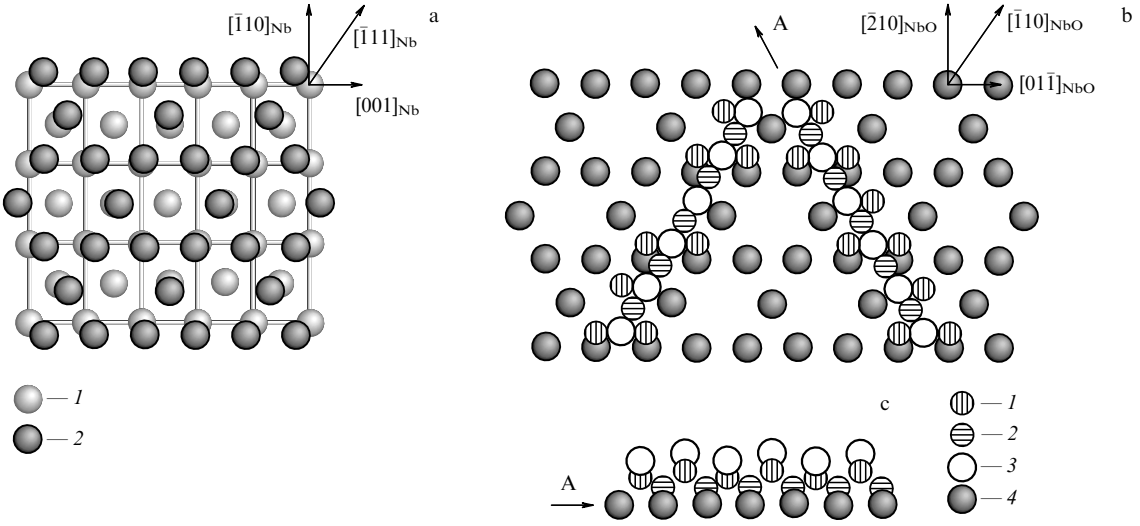

Figure 13. Model of an NbO layer on the Nb(110) surface: (a) hexagonal monolayer of Nb atoms belonging to the NbO layer (dark circles *2*) on the Nb(110) surface (gray circles *1*); (b) top view of a two-layer fragment: displaced rows of the NbO(111) structure on a hexagonal Nb monolayer, and (c) side view (section A) of the NbO/Nb_{hex} interface. Oxygen atoms O_{II} are shown as small white circles with a horizontal hatching (*1*); oxygen atoms O_I, small circles with a vertical hatching (*2*); niobium atoms in Nb^* rows, large open circles (*3*), and niobium atoms in the hexagonal monolayer, gray circles (*4*).

spectra and Nb 3d spectra, our team at ISSC, UB RAS (Ekaterinburg) estimated [55] the composition of this phase, which proved to be close to $NbO_{\sim 1.0}$ (Fig. 11c). It was found that the composition of the nanostructures on the Nb(110) surface is consistent with that of the NbO monoxide, but the chemical shift and, correspondingly, the chemical state of niobium atoms in this oxide differ from those characteristic of the bulk phase of the niobium monoxide. This fact can be related to the surface nature of the low-dimensional NbO structures. The estimation of the thickness of the NbO layer by the angle-resolved (AR) XPS in terms of the island model yields a value of ~ 5 Å [55], i.e., less than two niobium MLs in the composition of the oxide with an average surface coverage equal to 50%.

To determine the structural positions of the two nonequivalent forms of oxygen, O_I and O_{II}, on the NbO/Nb(110) surface, our team performed experiments [19, 27] on XPD emission of O 1s and Nb 3d photoelectrons (Fig. 12). The diffraction 2π pattern of scattering of Nb 3d photoelectrons in the layers of the NbO/Nb(110) interface on the whole replicates that observed for the pure Nb(110) face, demonstrating a twofold symmetry and the correspondence of the main diffraction maxima to the highest atomic density directions and planes of the bcc lattice of metallic niobium. Since the thickness of the NbO surface layer does not exceed 5 Å (with the probing depth of the XPD analysis being on the order of 30–50 Å), the contribution to the total XPD projection from the surface oxide is insignificant and mainly manifests itself in the case of grazing angles of photoemission. The resolution of this component (from the surface oxide) exhibits a sixfold symmetry with maxima at small angles, which indicates the presence of a hexagonal layer of niobium atoms at the Nb(110) surface, as in the case of the NbO(111) surface. The XPD pattern of Nb 3d electron photoemission calculated in the SSC-SW approximation for photoelectron scattering is given in Fig. 12c. Good agreement is revealed between the experimental and model patterns of the Nb 3d electron diffraction by the NbO/Nb(110) surface.

The situation is more complex in the case of the diffraction 2π pattern of O 1s photoemission from oxygen (Fig. 12b). At a high angular anisotropy ($\sim 60\%$), the XPD of O 1s photoelectrons is characterized by smeared maxima, two of which lie in the plane close to $Nb(\bar{1}10)$; one more (weaker) maximum lies in the Nb(001) plane. The existence of diffraction maxima in the XPD O 1s photoemission indicates the localization of at least part of the oxygen atoms below the niobium atoms. Using XPD calculations for O 1s photoelectrons, we established [19, 27] the positions of oxygen atoms on the niobium surface and suggested a structural model of the NbO/Nb(110) surface (Fig. 13). The model is based on the existence of two chemically nonequivalent forms of oxygen (O_I and O_{II}) in the proportion of $O_I/O_{II} \sim 2:1$, which were revealed using the XPD data on the structural positions of oxygen and STM images of the NbO/Nb(110) surface. The model comprises an Nb(110) surface, on top of which there is an Nb monolayer with a structure of the fcc packing of NbO(111) planes. The rows with ordered vacancies in the metal positions exist in this layer, as is the case in NbO monoxide. Then, there is a layer of oxygen and, further, rows (chains) of niobium atoms lying along the $NbO[\bar{1}10]$ direction. Approximately one-third of the oxygen atoms are localized in the structure of the Nb rows; the oxygen atoms are located between the metal atoms in the linear chains and lie below the Nb atoms. The remaining two-thirds of oxygen atoms are located in the immediate vicinity of Nb rows, forming an ordered structure of an oxygen sublattice, similar to that existing in fcc NbO.

Since we are dealing with the interface between two different lattices (bcc and fcc), the structure of the incompletely formed NbO surface layer becomes somewhat distorted: (1) the rows of niobium atoms have a finite length of 10 ± 1 atoms, being broken at a certain critical displacement of Nb atoms located in the rows from the optimum positions in the Nb(110) substrate because of the deflection of the $[\bar{1}10]_{fcc}$ and $[\bar{1}11]_{bcc}$ directions; (2) the Nb rows are displaced along the $[\bar{1}10]_{NbO}$ direction in such a way that each second Nb^* atom is located between two O_I atoms in the $NbO(\bar{2}11)$ plane, and the

remaining Nb^* atoms neighbor on only one O_I atom in this plane, and, finally, (3) half of the Nb^* atoms in the rows are 'lifted' relative to the hexagonal Nb monolayer by $\sim 0.6 \pm 0.2$ Å. The finite length of the NbO rows and the periodic structure arise as a result of the existence of anisotropic stresses between the two lattices $NbO(111)_{fcc}$ and $Nb(110)_{bcc}$. The structures that are formed on the surface can be considered as precursors of the epitaxial growth of NbO(111) layers on the Nb(110) surface.

A number of original results concerning the formation of surface oxygen structures on Nb(100) in the process of heat cleaning under UHV conditions and oxidation upon exposure of a crystal to oxygen at $T = 300$ and 900 K were obtained by the authors of Ref. [20], who used a combination of methods, such as AES, LEED, and STM. This appears to be the first work where an ideally pure (free of impurities) and structurally perfect niobium (100) surface has been obtained. To this end, the niobium single crystal was first cleaned using an Ar^+ ionic beam and annealed in UHV to $T = 2500$ K. In the range of annealing temperatures from 1970 to 2500 K, O (3×1), O (4×1), and O $c(2 \times 2)$ adsorption structures and a pure metal (1×1) structure were observed consecutively on the Nb(110) surface by the STM method (Fig. 14).

The O (3×1) structure is characterized by the existence of domains with boundaries extended along the [100] type directions. Such a domain structure reveals a tendency to ordering: each rectangular domain contains up to 11 unit cells in the direction of the shorter parameter. No long-period superstructure and corresponding superstructure reflections, similar to those observed for the adsorption structure on the Nb(110) face in Ref. [46], were revealed in the LEED patterns in Ref. [20].

According to Ref. [20], the tendency toward the formation of a superstructure is mainly related to the relaxation of the state of stress at the boundary between the epitaxial layers Nb(100) and NbO(100) with the fcc structure, where Nb[010] || NbO[110]. With increasing annealing temperature, part of the NbO molecules is evaporated and the O (3×1) structure is transformed into O (4×1), which is accompanied by an increase in the parameters of the quasiperiodic domain structure. With a further evaporation of NbO, structures of the O $c(2 \times 2)$ type with a completely disordered domain structure are formed on the base of the O (4×1) structure. Finally, the annealing at $T = 2500$ K leads to a complete removal of oxygen from the surface, where a (1×1) structure of the Nb(100) surface is observed. Notice that in earlier works [48, 71], the periodic oxide structures on Nb(100) were interpreted as an epitaxial layer of the $NbO_2(010)$ niobium dioxide.

The exposure of a pure Nb(100) surface to oxygen for 0.2–1.5 L at room temperature leads to the formation of O $c(2 \times 2)$ and O (1×1) structures. A further exposure to oxygen leads to the formation of cluster-like structures of NbO, NbO_2, and then Nb_2O_5 [20, 35]. Upon annealing in a UHV to $T = 870$ K, these structures are transformed into an O (3×1) structure. If the oxidation of the pure Nb(100) surface is performed at a higher temperature, e.g., at 900 K, then at the oxygen exposures of 0.2–1.5 L first an O $c(2 \times 2)$ structure and then an O (4×1) structure are consecutively formed. At exposures of 1.5–300 L, an O (3×1) structure is formed. A conclusion was made [20] that the epitaxial NbO monoxide grows on the surface in the process of molecular oxygen (O_2) deposition at enhanced temperatures owing to oxygen diffusion into the bulk of the metal. At room

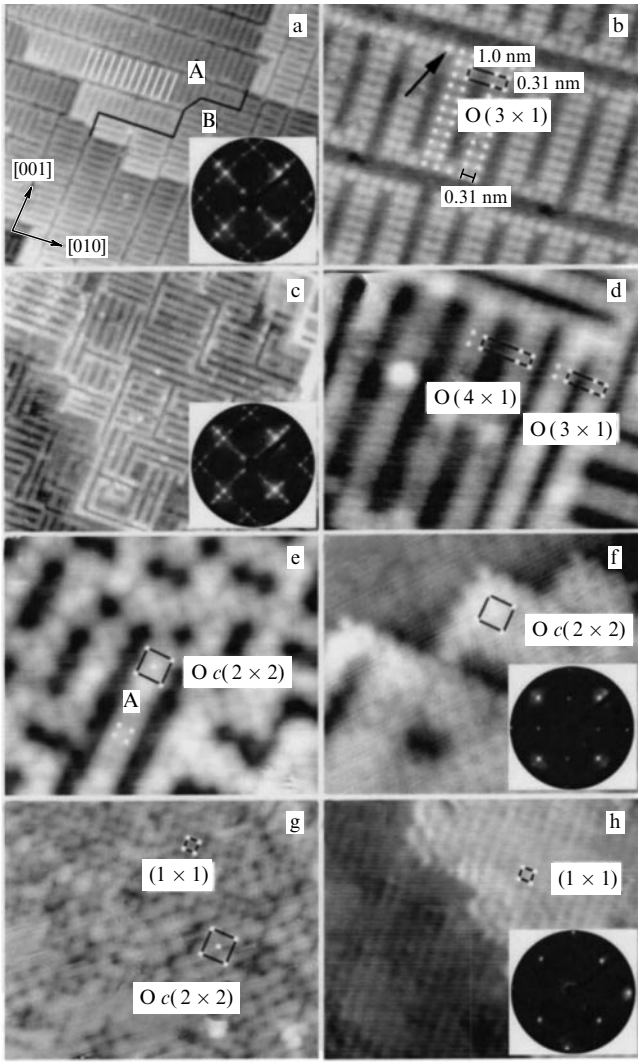

Figure 14. Results of the investigation of the O/Nb(100) surface by the STM and LEED methods [20]: (a, b) O (3×1) structure after annealing in a UHV at $T = 1970$ K, the image size is (a) 40×33 nm and (b) 8.5×7 nm; (c, d) O (4×1) structure after annealing in a UHV at $T = 2270$ K, the image size is (c) 40×33 nm and (d) 8.5×7 nm; (e, f) O $c(2 \times 2)$ structure after a sequential annealing in a UHV at $T = 2370$ K, the image size is 8.5×7 nm, and (g, h) transformation of the O $c(2 \times 2)$ structure into the (1×1) structure after annealing in a UHV at $T = 2500$ K, the image size is 8.5×7 nm.

temperature, amorphous oxides are formed on the surface, since under these conditions no oxygen diffusion into the bulk occurs, and the higher oxides are easily transformed into the amorphous state.

Consequently, the necessary conditions for the preparation of perfect (in composition and structure) surfaces of single-crystal niobium faces [e.g., NbO(110) and Nb(100)] and NbO_x structures on these faces are an ultrahigh vacuum and very high annealing temperatures. In this respect, the results of study [35] are demonstrative, where the vacuum in the experimental chamber was maintained at a level of 5×10^{-9} Pa, and the annealing temperature of the Nb(110) crystal (disk 6.2 mm in diameter and 1.2 mm thick) was varied from 2200 to 2700 K. The Auger electron spectroscopy of the surface showed that, after cleaning by Ar^+ ions and annealing at $T = 2200$ K, the higher Nb_2O_5 and NbO_2 oxides are removed from the surface, but oxygen in the form of NbO remains on it. A prolonged cyclic annealing of the crystal

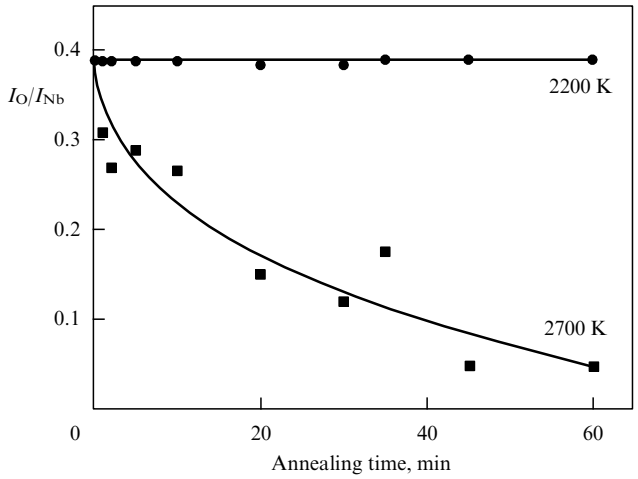

Figure 15. Variation in the oxygen concentration (I_O/I_{Nb} ratio according to AES data) on the Nb(110) surface in the process of annealing a crystal in a UHV at temperatures of 2200 and 2700 K [35].

(using the flash method with a cycle duration of 2 min) to $T = 2200$ K for 1 h does not lead to a change in the oxygen concentration on the surface (Fig. 15). An analogous treatment with flash annealing to $T = 2700$ K decreases the oxygen concentration on the surface by a factor of eight, to ~ 5 at.%. The LEED patterns indicate the existence of an NbO(111) monolayer on the Nb(110) surface after annealing at $T = 2273$ K and of a (1×1) structure of the Nb(110) surface after prolonged annealing at $T = 2700$ K.

Thus, the oxygen-induced superstructures on single-crystal Nb surfaces can be formed in two ways: as a result of high-temperature annealing in a UHV or as a result of oxygen adsorption onto a pure niobium surface at lower temperatures.

The data obtained in recent years have made it possible to study the new oxygen-containing structures in much detail; in particular, these data showed the important role of the competition between the segregation of oxygen dissolved in the bulk of the crystal and the evaporation of oxides from the surface. It is the oxygen-induced layers of the NbO_x type on the close-packed niobium (110) and (100) surfaces that have been studied in the most details. Although their atomic structure has not been established exactly, it is assumed that they are related to the NbO monoxide, and the corresponding orientation relationships for matching the structures of the oxide and the metallic substrate are employed. It should be noted that the structure of the oxygen-induced layer on the Nb(110) face is more complex; upon its formation, the substrate suffers a reconstruction caused by the noncoincidence of the symmetries and parameters of the conjugating planes of niobium and the oxide, resulting in the formation of a long-period superstructure accompanying the relaxation of the state of stress at the interface. In the case of the oxygen-induced layers on the Nb(100) face, no reconstruction occurs, since the coincident planes have the same symmetry. No long-period structures are formed on the Nb(100) face; here, only a tendency to the formation of a quasiperiodic domain structure reveals itself; it is obvious that the stresses that are accumulated at the interface between the less-close-packed $NbO_x(100)/Nb(100)$ planes are not so much as in the case of the $NbO_x(111)/Nb(110)$ interface.

It seems that for further studies, in particular, for the establishment of the atomic structure of adsorption layers and for an analysis of the energy content and stability of these structures, *ab initio* calculations can be of great importance. As the first objects here, oxygen-induced structures on the Nb(100) face can be employed as the simplest ones. For analyzing the adsorption structures on the Nb(110) face, additional experimental studies are required in order to clarify the structural states of the $NbO_x(111)/Nb(110)$ interface.

4.3 Adsorption of nitrogen, hydrogen, and other gases on the niobium surface

The adsorption of N_2 on an Nb(110) surface was studied at $T = 80$ and 20 K using high-resolution electron energy loss spectroscopy (HREELS) [60]. It was shown that nitrogen is actively chemisorbed on Nb(110) at $T = 80$ K with the formation of NbN and atomic chemisorbed forms, such as Nb ≡ N. At 20 K, a molecular chemisorption of N_2 occurs; after the saturation of the surface by these states, nitrogen continues physisorbing on the Nb(110) surface in the molecular form. It can be expected that at room temperature the situation will be closer to that observed with the adsorption of N_2 at $T = 80$ K, where an NbN nanolayer is formed and atomic chemisorption of nitrogen occurs. The key role in such experiments is played by the purity of the niobium surface. The presence of oxygen or oxide phases on the surface reduces the adsorption activity of nitrogen by an order of magnitude.

In Ref. [74], the dissociative chemisorption of nitrogen on an Nb(100) surface was studied. At room temperature, the pure Nb (1×1) structure is transformed into a disordered structure with the formation of local fragments of an N (2×1) structure upon exposure to 0.4 L; a further adsorption of N_2 leads to the formation of cluster-like NbN structures on the surface. At $T = 620$ K, the pure (1×1) structure first transforms into an N $c(2 \times 2)$ structure (at 0.6 L) and then into an N (5×5) structure (at 10 L). The latter is transformed into an N (1×5) structure upon annealing under UHV conditions or at a nitrogen pressure of 10^{-7} Pa and $T = 620$ K.

Numerous studies have been devoted to the investigation of the interaction of an Nb surface with hydrogen. As is known, interstitial solid solutions (with a hydrogen concentration to 10 at.%) and hydride-like $NbH_{0.7-1.0}$ phases are formed in the Nb–H system. The solubility of hydrogen in Nb at 20 °C is 104 g cm^{-3}; at 500 °C, 74.4 g cm^{-3}, and at 900 °C, 4.0 g cm^{-3}. The process of hydrogenation is reversible; upon heating, especially in a vacuum, the hydrogen is liberated; this is used for refining Nb from hydrogen. Niobium is considered a promising material for a hydrogen storage. The possibility of employing niobium membranes for the production of pumps for the evacuation of hydrogen and its isotopes from fusion reactors is under discussion [87]. The results of experiments have evidenced that the trapping of low-energy deuterium ions by niobium depends strongly on the state of the surface. Thus, the existence of an oxide layer on the niobium surface increases the trapping coefficient severalfold.

The surface structures arising on Nb(100) upon adsorption of hydrogen ($T = 300$ K) have been studied in Ref. [79] by the STM method. It was shown that the (1×1) structure of a pure niobium surface is retained up to exposures $L(H_2) = 8$ L, whereupon they are transformed into cluster-like fragments of niobium hydride at $L(H_2) = 50$ L. The latter are easily decomposed upon vacuum annealing for

$T \geqslant 450$ K, and the hydrogen atoms diffuse into the bulk of the niobium, forming an Nb : H solid solution. Upon cooling to room temperature, the hydrogen atoms diffuse from the bulk to the surface and accumulate in the subsurface layer. This leads to an expansion of the niobium lattice under the surface; as a result, a (1×1) structure is formed on the surface, consisting of niobium atoms in the form of small islands with linear defects that compensate for the deformation (geometrical distortion) of the niobium lattice under the surface.

Two models have been suggested to describe the mechanism of niobium interaction with hydrogen. In the first model, it is assumed that a layer of a hydride is formed ($T \leqslant 350$ K) on the niobium surface, which controls the transfer of hydrogen through the surface into the bulk of the metal [64, 88]. The other — the so-called two-layer model [62] — assumes that the hydrogen diffusion through the surface is determined by the subsurface layer saturated by hydrogen. According to this model, the hydrogen in surface interstitial sites is most stable energetically and serves as a barrier between the chemisorbed hydrogen and the bulk of the metal up to a critical temperature of about 473 K. According to Ref. [78], the hydrogen sites under the niobium surface are close in their nature to tetrahedral positions that hydrogen occupies in the NbH hydride. In Ref. [80], theoretical estimates of the subsurface sites of hydrogen on the Nb(100) face have been performed.

As examples of the investigations into adsorption of other gases on the niobium surface, let us note the theoretical studies [89] and [90], where CO, CN/Nb(110) and NH_3/Nb(100) systems were considered, respectively. Investigations of the stability of the molecular adsorption of CO and CN (stability against dissociative decomposition) on the surface of a number of 4d metals, including the Nb(110) surface, disclosed [89] that the CO molecules are more stable on the surfaces of 4d metals on the right-hand side of the Periodic Table (beginning from Tc), while the CN molecules, on the contrary, are more stable on those metals at the beginning part of the 4d row (Zr, Nb, and Mo).

In Ref. [90], the authors simulated the process of adsorption and dissociation of ammonia (NH_3) molecules and their derivatives on two types of surface centers: over Nb atoms (on-top sites), and between four Nb atoms over an octahedral interstice (4-fold-hollow site). The calculations demonstrated that molecular chemisorption is an energetically favorable process for all fragments of the decomposing ammonia; however, the dissociation process itself depends on the molecular positions at the surface. Thus, the dissociation of ammonia molecules is improbable in the on-top centers. Upon the localization at 4-fold-hollow centers, the $NH_3 \rightarrow NH_2 + H$ decomposition occurs slowly, but this process accelerates after the formation of NH_2. The dissociation products diffuse into the bulk of niobium, forming nitrides and changing the composition of the surface.

The adsorption of water on the Nb(110) surface was investigated in Ref. [91] using ultraviolet photoelectron spectroscopy. It was revealed that the H_2O molecules decompose partly on the niobium surface into OH^- and H^+; in this case, both linear and inclined configurations of the Nb–O–H bonds can arise.

5. Pure surfaces of group IV–VI d-metals and surface oxide structures

The surfaces of transition metals of groups IV–VI and of the adsorption systems based on these metals have been investigated in numerous studies (see, e.g., Ref. [92]).

In particular, the atomic and electronic structures of the surface of group IV–VI d-metals, including the effects of relaxation contraction (expansion) of surface layers, have been studied in detail using the computational methods of quantum theory (Table 6). Systematic investigations of the interlayer relaxation of the surface of a number of 4d metals have been performed in terms of the density-functional theory (DFT) [93] based on most close-packed faces of the metals as an example. It has been shown that the magnitudes of the relaxation contraction of the first two layers of the Zr(0001), Nb(110), and Mo(110) surfaces are no more than 2–6% of the interlayer spacing in the bulk of metals. In the row of 4d metals, the level of relaxation reduces consecutively from $\sim 4\%$ for Y(0001) to almost zero in the case of Ag(111).

Based on the group V d-metals (V, Nb, and Ta) as an example, there has been revealed [93–98] an enhancement of the relaxation effects upon transition from the low-index close-packed (110) faces to more 'open' (100) surfaces and further to (111). Thus, the relaxation increases in the case of tantalum from 5% for Ta(110) to 27% for Ta(111); in the case of niobium, as was noted above, the relaxation grows from 5.8% for Nb(110) to 24.8% for Nb(111). The relaxation contraction (expansion) is not limited by the first two layers.

Table 6. Magnitudes of relaxation contraction of surface layers for group IV–VI d-metals: experiment and calculations.

Element	Contraction, %	References	Element	Contraction, %	References	Element	Contraction, %	References
^{22}Ti			**^{23}V**			**^{24}Cr**		
Ti(0001)	6.8 ± 1	[95]	V(110)	5	[97]	Cr(100)	3.7	[94]
	7.7	[96]	Expt.	3.3	[97]			
Ti(111)	7.1	[96]	V(100)	11	[94]			
^{40}Zr			**^{41}Nb**			**^{42}Mo**		
Zr(0001)	2.8	[93]	Nb(110)	1.9	[93]	Mo(110)	1.6	[93]
	6 ± 2	[100]		5.8	[83]	Expt.	1.6	[93]
	6.3	[96]	Nb(100)	4.7	[93]	Mo(100)	4.4	[93]
Expt.	2.54 ± 0.05	[99]		11.7	[83]	Expt.	11.5	[93]
Zr(111)	5.9	[96]	Nb(111)	24.8	[83]			
^{72}Hf			**^{73}Ta**			**^{74}W**		
	No data		Ta(110)	5	[98]	W(110)	0.8	[101]
			Ta(100)	14	[98]		3.1	[102]
			Expt.	11 ± 2	[99]	W(100)	4	[101]
			Ta(111)	27	[98]	Expt.	3.13	[101]

Table 7. Energy shifts (S) of the surface states of the XPS lines attributed to the inner shells of group IV–VI d-metals.

Element	Shift, eV	References	Element	Shift, eV	References	Element	Shift, eV	References
^{22}Ti Ti 2p Ti(0001)	$S \sim +0.5$	[114]	**^{23}V** V 2p	No data		**^{24}Cr** Cr 2p Cr(polycryst.)	$S = -0.8$	[119]
^{40}Zr Zr 3d Zr(0001)	$S \sim 0.0$	[115]	**^{41}Nb** Nb 3d Nb(100)	$S_1 = +0.49$ $S_2 = +0.13$	[21] [21]	**^{42}Mo** Mo 3d Mo(110)	$S_1 = -0.33$ $S_2 = -0.14$	[21] [21]
^{72}Hf Hf 4f Hf(polycryst.) Hf(0001)	$S = +0.42$ $S = +0.40$	[21] [103]	**^{73}Ta** Ta 4f Ta(111) Ta(100) Ta(110) 	$S_1 = +0.40$ $S_2 = +0.22$ $S_3 = +0.06$ $S_1 = +0.74$ $S_2 = +0.14$ $S_1 = +0.90$ $S_2 = +0.15$ $S = +0.25$ $S_1 = +0.28$ $S_2 = +0.01$	[117] [117] [117] [21] [21] [118] [118] [103] [117] [117]	**^{74}W** W 4f W(111) W(100) W(110) W(110)	$S_1 = -0.44$ $S_2 = -0.11$ $S_1 = -0.36$ $S = -0.35$ $S = -0.32$	[116] [116] [21] [120] [121]

For the Nb, V, and Cr surfaces, it has been established [83, 94] that the relaxation decays harmonically upon moving into the bulk of the metal: the first two monolayers of the Cr(100) face [94] contracted by 3.7%; the second and third layers, on the contrary, expanded by 4.4%, and the third and fourth layers again contracted by 0.2%, i.e., the relaxation effects for the Cr(100) surface involve 3–4 layers. For more 'open' surfaces, e.g., for Nb(111), the relaxation involves ten or an even greater number of layers.

Experimentally, the relaxation contraction (expansion) of the surface layers of d metals was studied by the LEED and XPD methods; the corresponding data are given in Table 6.

Another important characteristic of d-metal surfaces is the transformation of the electronic structure of the uppermost layers relative to that in the bulk of the metals. Here, two interesting features can be singled out: the appearance of additional (so-called 'surface') states near the Fermi level, and the 'surface' core-level shifts (SCLSs). The theory and spectroscopy of these phenomena have been described in detail in the generalizing studies [103, 104]; data on the surface shifts of 2p, 3d, and 4d electron levels of group IV–VI transition metals are summarized in Table 7.

It was established that a shift of the surface states toward greater binding energies relative to the 'bulk' band of the crystal is characteristic for group IV–VI d-metals; in the case of molybdenum and tungsten, on the contrary, the energy shift occurs toward lower values of E_b.

The atomic structure of pure surfaces of the d-metals considered was studied by the STM method. The STM image of the (1×1) lattice of the pure Nb(100) face was for the first time obtained in Ref. [20] (Fig. 14g). STM images of the Mo(112) surface were presented (also for the first time) in Ref. [105]. The authors of Ref. [106] obtained STM images and constructed theoretical models of pure Mo(112) and Mo(111) surfaces; in Ref. [107], they studied the Ta(211) surface. The pure close-packed Mo(110) face was prepared and studied by the STM method in Ref. [108]. The pure close-packed tungsten faces W(110) and W(100) are traditionally utilized as substrates for depositing monolayer films of various materials; these surfaces have been well studied and demonstrate the potential of the STM method. Chromium occupies a special site in the row of the d-metals under consideration owing to its magnetic properties (antiferromagnetism and spin-density waves); its surface was also studied in a number of interesting studies [109–112].

Earlier, we discussed ordered oxygen-induced nanostructures on the niobium (110) and (100) surfaces. Similar structures have been revealed on the surfaces of some other transition metals. Figure 16 displays STM images of oxide structures on the surfaces of d-metals entering groups V and VI of the Periodic Table. To the best of our knowledge, however, no analogous STM studies have been performed on group IV metals (Ti, Zr, and Hf). This is apparently explained by the capability of these hcp metals to adsorb oxygen and rapidly form structures of higher oxides on the surface [33]. It is hardly possible to remove these higher oxides from their surfaces using high-temperature vacuum annealing, as is performed, for example, for niobium and tungsten, since Ti and Zr undergo polymorphic phase transitions ($\alpha \rightarrow \beta$) at temperatures of 1155.5 and 1135 K, respectively. No STM images of oxygen structures on these faces in Ta are available in the literature; the image given in Fig. 16 corresponds, according to the authors of Ref. [100], to a pure Ta(211) face.

In the case of vanadium, a periodic $c(6 \times 2)$ structure was observed (see Fig. 16) on the V(100) surface in the adsorption of oxygen at $T = 520$ K [97]. Due to a strong vanadium–oxygen interaction, the metallic lattice of the first surface layer undergoes significant distortions, forming threefold- and fourfold-coordinated interstices in the metal lattice, in which oxygen is chemisorbed to a surface coverage $\vartheta_O = 0.5$ ML.

In Ref. [108], surface oxygen-induced structures were created on the Mo(110) face by the exposure of the crystal to oxygen at a temperature of 1300 K and a pressure of 4×10^{-6} Pa (using several cycles) with a subsequent annealing in a UHV. Two variants of surface structures have been revealed: traditional O $p(2 \times 1)$ structures (domains of two types), and more complex structures in the form of discrete large protrusions and short zigzagging protrusions (see Fig. 16). The last ones are interpreted in Ref. [108] as transient states in the 'site conversion' of adsorbed oxygen atoms from the 'long-bridge' sites between two tantalum atoms into more energetically preferred positions between three metal atoms (threefold-coordinated sites) in the

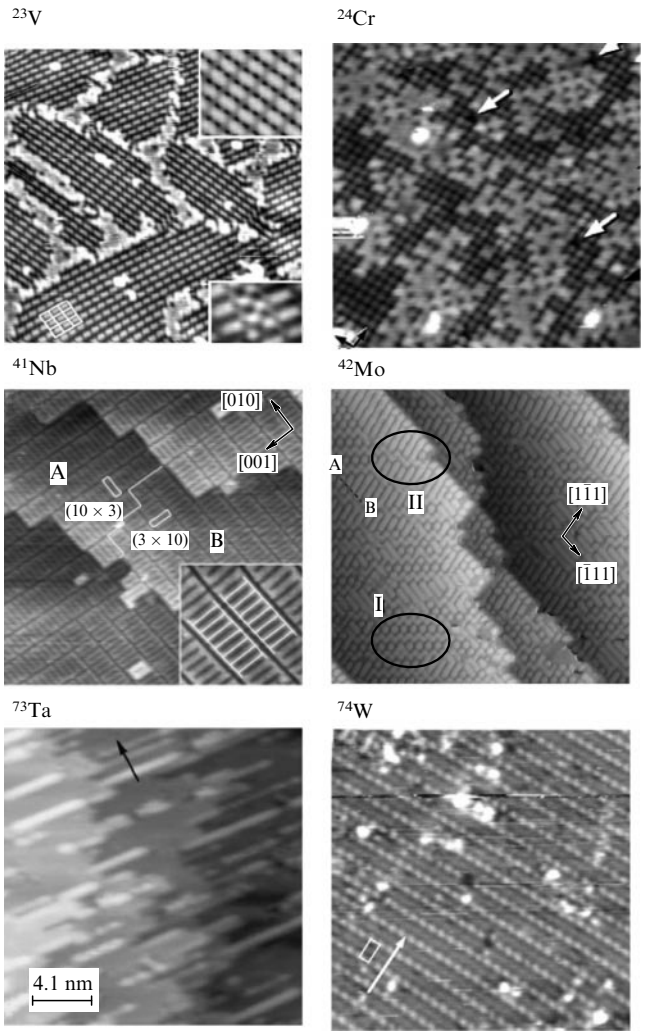

Figure 16. Oxygen-induced adsorption structures on the surfaces of group V–VI d-metals: V(110) [97]; Cr(100) [112]; Nb(100) [48]; Mo(100) [108]; Ta(211) [100], and W(110) [113].

Mo(110) lattice. On the more open Mo(112) face, the oxygen chemisorption provokes a reconstruction of the surface with the formation of linear $p(2 \times 3)$ structures; according to Ref. [105], these are precursor states for the epitaxial growth of an MoO_2 layer on Mo(112).

The oxygen adsorption on tungsten W(110) faces was studied by Irving Langmuir as long ago as 1913. To date, the periodic structures on tungsten surfaces have been characterized in detail by the LEED, STM, and other methods [113]. Oxygen forms four different surface structures on W(110), depending on the adsorption conditions (exposure, temperature, oxygen pressure, etc.). An O (2×1) structure forms on the W(110) surface at the coverage $\Theta_O = 0.5$ ML; at coverages $\vartheta_O = 0.75$ and 1.00 ML, O (2×2) and O (1×1) structures, respectively, are formed. In Ref. [113], one more periodic O/W(110) structure was found to exist at $\vartheta_O = 0.4$ ML; its STM image is also given in Fig. 16.

The authors of Ref. [112] observed the formation of $\sim 17\%$ vacancies in the metallic sublattice of a Cr(100) surface oxygen-covered to 1 ML. The oxygen atoms, chemisorbed as a result of O_2 adsorption ($T = 300$ K) or segregated from the bulk of Cr upon high-temperature annealing in a vacuum, occupy all available hollow sites in the first surface monolayer, including positions near the vacancies of the chromium lattice. It is stated in Ref. [112] that the formation of vacancies is due to the specific features of the electronic structure of the chromium surface rather than to stresses that arise in the surface layer upon oxygen incorporation. Figure 16 displays the O/Cr(100) surface after oxygen adsorption to a coverage of 2 L. Light regions of a pure chromium surface with isolated 'dints', and large regions where a $p(1 \times 1)$ superstructure exists can be seen. As oxygen (O_2) exposure increases, the area of the $p(1 \times 1)$ regions also increases.

6. Conclusions

It should be noted in conclusion that to date vast and very interesting data have been accumulated concerning the preparation and thorough investigation of pure surfaces of transition d-metals and low-dimensional surface nanostructures that are formed on these metals upon adsorption, due to impurity segregation from the bulk of the metal, and as a result of other processes.

In this review, we attempted to consider, using the example of a niobium surface and surface oxide nanostructures, both the advances achieved and the problems that exist in the field of preparation and experimental and theoretical investigations of these systems; for comparison, we also briefly considered the surfaces of some related group IV–VI d-metals.

The data available suggest that the preparation of a chemically pure and structurally perfect niobium surface is quite a complex problem. At the final stage of the preparation of the niobium surface upon high-temperature vacuum annealing, surface oxide structures are formed due to the segregation of impurity oxygen from the bulk of the niobium.

Therefore, experimental investigations of the structure and properties of oxides or, to be precise, of quasiperiodic $NbO_{x\sim1.0}$ nanostructures on the surface of this metal are of great importance. We mean both NbO structures on Nb(100) and Nb(110) faces of single-crystal niobium and the epitaxial thin niobium films. Notice that to date there is no common opinion on the nature and mechanisms of the formation of periodic NbO structures on niobium. Thus, some researchers think that the oriented NbO(111) nanocrystals grow on the metal surface due to oxygen diffusion from the bulk of the niobium crystal (upon heating in a vacuum) and that the directions and dimensions of the crystals are determined by the lattice misfit between the fcc NbO film and bcc Nb(110) substrate; other authors consider the arising structures as oxygen-induced quasiordered structures on the metal surface that are precursors for the growth of an epitaxial $NbO_x(111)$ layer on the Nb(110) or Nb(100) substrates. In these surface structures, the niobium atoms are characterized by nearest surroundings and chemical bonds similar to those characteristic of NbO, but exhibit some differences (e.g., in the electronic structure and properties) from the bulk niobium monoxide due to the size effect.

At present, the main methods of investigating the pure niobium surface and surface structures on niobium (and related systems) are scanning tunneling microscopy (STM), X-ray photoelectron spectroscopy (XPS), low-energy electron diffraction (LEED), and Auger electron spectroscopy (AES). In the analysis of structural positions of oxygen on the Nb(110) surface, the method of X-ray photoelectron diffraction (XPD) with the resolution of oxygen chemical states is also very efficient. On the whole, these techniques yield

detailed information on the composition, structure, and topology of NbO/Nb(110) and NbO/Nb(100) surfaces. The oxide structures on other faces of single-crystal niobium have been studied in less detail; also, work on the formation of periodic structures of nitrides, carbides, and some other compounds on the niobium surface is rare.

In the field of computer simulation of the surfaces of niobium and other transition metals, the situation is opposite to that observed in the experimental field. To date, a large sequence of detailed calculations of ideal surfaces of metals has been performed using the *ab initio* methods of the energy-band theory, and many important characteristics, such as the degree of relaxation contraction (expansion) of surface layers and the densities of electron states and the distributions of charge density near the surface, have been estimated. At the same time, calculations of oxide and other nanostructures on the surface of niobium and related group IV–VI d-metals are virtually absent. Therefore, a detailed analysis of both experimentally prepared and hypothetical oxide and related nanostructures on the surface of d-metals, which is important for a clear understanding of the microscopic mechanisms of their formation and growth, is, in our opinion, the next task of the theory.

Acknowledgments

We are very grateful to N I Medvedeva, E V Shalaeva, and I R Shein for the fruitful discussions. The work was supported in part by the Russian Foundation for Basic Research, project nos. 08-03-00043-a and 10-03-96047-Ural.

References

1. Singer W *Physica C* **441** 89 (2006)
2. Corato V et al. *Supercond. Sci. Technol.* **17** S385 (2004)
3. Gol'tsman G N et al. *Appl. Phys. Lett.* **79** 705 (2001)
4. Shirakashi J et al. *Jpn. J. Appl. Phys.* **37** 1594 (1998)
5. Töpfer H, Harnisch T, Uhlmann F H *J. Physique IV* **6** (C3) C3-345 (1996)
6. Grant J T, Briggs D (Eds) *Surface Analysis by Auger and X-ray Photoelectron Spectroscopy* (Chichester, UK: IM Publications, 2003)
7. Briggs D, Seah M P (Eds) *Practical Surface Analysis by Auger and X-ray Photoelectron Spectroscopy* (Chichester: Wiley, 1983) [Translated into Russian (Moscow: Mir, 1987)]
8. Shalaeva E V, Kuznetsov M V *Zh. Strukt. Khim.* **44** 518 (2003) [*J. Struct. Chem.* **44** 465 (2003)]
9. Woodruff D P *Surf. Sci. Rep.* **62** 1 (2007)
10. Fadley C S et al. *J. Electron Spectrosc. Relat. Phenom.* **68** 19 (1994)
11. Mironov V L *Osnovy Skaniruyushchei Zondovoi Mikroskopii* (Fundamentals of Scanning Probe Microscopy) (Moscow: Tekhnosfera, 2004)
12. Cohen S H, Lightbody M L (Eds) *Atomic Force Microscopy/ Scanning Tunneling Microscopy 3* (New York: Kluwer Academic/ Plenum Publ., 1999)
13. Massalski T B (Ed.-in-Chief), Okamoto H, Subramanian P R, Kacprzak L (Eds) *Binary Alloy Phase Diagrams* 2nd ed., Vol. 3 (Materials Park, Ohio: ASM Intern., 1990)
14. Kaim R E, Palmer D W *Philos. Mag. A* **40** 279 (1979)
15. Nowick A S, Berry B S *Anelastic Relaxation in Crystalline Solids* (New York: Academic Press, 1972)
16. Fromm E, Gebhardt E V (Hrsg.) *Gase und Kohlenstoff in Metallen* (Berlin: Springer-Verlag, 1976) [Translated into Russian (Moscow: Metallurgiya, 1980)]
17. Rao C N R, Rao G V *Transition Metal Oxides* (Washington: Natl. Bureau of Stands, 1974)
18. Linetskii B L et al. *Bezokislitel'nyi Nagrev Redkikh Metallov i Splavov v Vakuume* (Nonoxidation Heating of Rare Metals and Alloys in Vacuum) (Moscow: Metallurgiya, 1985)
19. Razinkin A S, Thesis for Candidate of Chemical Sciences (Ekaterinburg: Institute for Solid State Chemistry, Ural Branch of the Russian Academy of Sciences, 2009)
20. An B et al. *Phys. Rev. B* **68** 115423 (2003)
21. Lo W-S et al. *Phys. Rev. B* **51** 14749 (1995)
22. Aldén M, Skriver H L, Johansson B *Phys. Rev. Lett.* **71** 2449 (1993)
23. Fang B-S, Lo W-S, Chen H-H *Phys. Rev. B* **47** 10671 (1993)
24. Colera I, Rey S, Segovia J L *Surf. Sci.* **251/252** 851 (1991)
25. Lo W-S et al. *Surf. Rev. Lett.* **5** 1035 (1998)
26. Xu M L, Tong S Y *Phys. Rev. B* **31** 6332 (1985)
27. Razinkin A S, Shalaeva E V, Kuznetsov M V *Fiz. Met. Metalloved.* **106** (1) 59 (2008) [*Phys. Met. Metallogr.* **106** (1) 56 (2008)]
28. Louie S G et al. *Phys. Rev. Lett.* **37** 1289 (1976)
29. Louie S G et al. *Phys. Rev. B* **15** 5627 (1977)
30. Methfessel M, Hennig D, Scheffler M *Phys. Rev. B* **46** 4816 (1992)
31. Lekka Ch E et al. *Phys. Rev. B* **68** 035422 (2003)
32. Shein K I et al. *Fiz. Met. Metalloved.* **102** 648 (2006) [*Phys. Met. Metallogr.* **102** 604 (2006)]
33. Kuznetsov M V, Shalaeva E V, Medvedeva N I, Ivanovskii A L *Khimiya Poverkhnosti Razdela Titan–Gaz: Eksperiment i Teoriya* (Chemistry of Titanium–Gas Interface: Experiment and Theory) (Ekaterinburg: Inst. Khimii Tverdogo Tela UrO RAN, 1999)
34. Fromm E, Mayer O *Surf. Sci.* **74** 259 (1978)
35. Franchy R, Bartke T, Gassmann P *Surf. Sci.* **366** 60 (1996)
36. Ptushinskii Yu G, Chuikov B A *Poverkhnost* (9) 5 (1992)
37. Dvoretski Z et al. *Poverkhnost* (1) 40 (1987)
38. Bosov V S et al. *Poverkhnost* (2) 126 (1983)
39. Ishchuk V A, Makhkamov M I, Ptushinskii Yu G *Poverkhnost* (3) 48 (1988)
40. Ishchuk V A et al. *Poverkhnost* (10–11) 24 (1994)
41. Pantel R, Bujor M, Bardolle J *Surf. Sci.* **62** 589 (1977)
42. Farrell H H, Strongin M *Surf. Sci.* **38** 18 (1973)
43. Lo W-S et al. *Surf. Rev. Lett.* **4** 651 (1997)
44. Usami S, Tominaga N, Nakajima T *Vacuum* **27** 11 (1977)
45. Uehara Y et al. *Surf. Sci.* **472** 59 (2001)
46. Sürger Ch, Schöck M, v. Löhneysen H *Surf. Sci.* **471** 209 (2001)
47. Arfaoui I, Cousty J, Safa H *Phys. Rev. B* **65** 115413 (2002)
48. Li Y et al. *J. Appl. Phys.* **89** 4772 (2001)
49. Arfaoui I et al. *J. Appl. Phys.* **91** 9319 (2002)
50. Arfaoui I, Cousty J, Guillot C *Surf. Sci.* **557** 119 (2004)
51. Matsui F et al. *Czech. J. Phys.* **56** (1) 61 (2006)
52. Shalaeva E V, Kuznetsov M V *Fiz. Met. Metalloved.* **96** (5) 79 (2003) [*Phys. Met. Metallogr.* **96** 514 (2003)]
53. Ishchuk V A et al. *Fiz. Tverd. Tela* **23** 1282 (1981)
54. Razinkin A S, Shalaeva E V, Kuznetsov M V *Izv. Ross. Akad. Nauk Ser. Fiz.* **72** 1395 (2008) [*Bull. Russ. Acad. Sci. Phys.* **72** 1318 (2008)]
55. Kuznetsov M V, Razinkin A S, Shalaeva E V *Zh. Strukt. Khim.* **50** 536 (2009) [*J. Struct. Chem.* **50** 514 (2009)]
56. Hu Z P et al. *Solid State Commun.* **71** 849 (1989)
57. Hayoz J et al. *Appl. Phys. A* **71** 615 (2000)
58. Colera I, Rey S, de Segovia J L *Vacuum* **41** 224 (1990)
59. Colera I, Rey S, de Segovia J L *Surf. Sci.* **251 – 252** 851 (1991)
60. Franchy R, Bartke T U *Surf. Sci.* **322** 95 (1995)
61. Crawford P, Hu P *J. Chem. Phys.* **126** 194706 (2007)
62. Lagos M, Rogan J, Schuller I K *Phys. Rev. B* **44** 3380 (1991)
63. Lagos M, Schuller I K *Phys. Rev. B* **32** 5477 (1985)
64. Dienes G J, Strongin M, Welch D O *Phys. Rev. B* **32** 5475 (1985)
65. Smith R J *Phys. Rev. B* **21** 3131 (1980)
66. Kim S-W et al. *Phys. Rev. B* **38** 5716 (1988)
67. Kim S-W, Sohn K S *Phys. Rev. B* **40** 1003 (1989)
68. Fang B-S et al. *Phys. Rev. B* **50** 11093 (1994)
69. Fang B-S, Ballentine C A, Erskine J L *Phys. Rev. B* **38** 4299 (1988)
70. Lo W-S et al. *Surf. Rev. Lett.* **5** 1035 (1998)
71. Li Y et al. *Mater. Characterization* **48** 163 (2002)
72. Ma Q et al. *J. Appl. Phys.* **96** 7675 (2004)
73. Hüger E et al. *Europhys. Lett.* **83** 26001 (2008)
74. An B et al. *Phys. Rev. B* **73** 205401 (2006)
75. Farrell H H, Strongin M *Surf. Sci.* **38** 31 (1973)
76. Dickey J M *Surf. Sci.* **50** 515 (1975)
77. Fang B-S, Ballentine C A, Erskine J L *Phys. Rev. B* **36** 7360 (1987)
78. Li Y, Erskine J L, Diebold A C *Phys. Rev. B* **34** 5951 (1986)
79. An B et al. *Jpn. J. Appl. Phys.* **43** 4502 (2004)
80. Romero A H, Schuller I K, Ramirez R *Phys. Rev. B* **58** 15904 (1998)

81. Ollonqvist T et al. *Surf. Sci.* **402** 678 (1998)
82. Daccà A et al. *Appl. Surf. Sci.* **126** 219 (1998)
83. Lekka Ch E, Papaconstantopoulos D A *Surf. Sci.* **601** 3937 (2007)
84. King B R et al. *Thin Solid Films* **192** 351 (1990)
85. Hatano Y et al. *Phys. Scripta* **T108** 14 (2004)
86. Grundner M, Halbritter J *Surf. Sci.* **136** 144 (1984)
87. Evanov A A et al. *J. Nucl. Mater.* **271 – 272** 330 (1999)
88. Strongin M et al. *Phys. Rev. B* **26** 2715 (1982)
89. Crawford P, Hu P *Surf. Sci.* **601** 341 (2007)
90. Cheng H et al. *J. Phys. Chem.* **100** 9800 (1996)
91. Colera I et al. *Surf. Sci.* **292** 61 (1993)
92. Taft C A et al. *Intern. Rev. Phys. Chem.* **18** (2) 163 (1999)
93. Kádas K et al. *Surf. Sci.* **600** 395 (2006)
94. Bihlmayer G, Asada T, Blügel S *Phys. Rev. B* **62** R11937 (2000)
95. Teeter G, Erskine J L *Phys. Rev. B* **61** 13929 (2000)
96. Feibelman P J *Phys. Rev. B* **53** 13740 (1996)
97. Koller R et al. *Surf. Sci.* **512** 16 (2002)
98. Kiejna A *Surf. Sci.* **598** 276 (2005)
99. Titov A, Moritz W *Surf. Sci. Lett.* **123** L709 (1982)
100. Yamamoto M et al. *Surf. Sci.* **387** 300 (1997)
101. Batirev I G et al. *Surf. Sci.* **417** 151 (1998)
102. Oguchi T *Surf. Sci.* **438** 37 (1999)
103. Hüfner S *Photoelectron Spectroscopy*: *Principles and Applications* (Berlin: Springer-Verlag, 1995)
104. Jakobi K "Surface core-level shift data. 3.1.2.5", in *Springer Materials, The Landolt-Börnstein Group III Condensed Matter, Numerical Data and Functional Relationships in Science and Technology* Vol. 24b *Electronic and Vibrational Properties* (Ed. G Chiarotti) (Berlin: Springer-Verlag), doi: 10.1007/10086058_17
105. Schroeder T et al. *Phys. Rev. B* **65** 115411 (2002)
106. Yakovkin I N et al. *Surf. Sci.* **600** L240 (2006)
107. Kuchowicz M, Stepanovsky S, Kolaczkiewicz J *Surf. Sci.* **600** 1600 (2006)
108. Okada A, Yoshimura M, Ueda K *Surf. Sci.* **601** 1333 (2007)
109. Schäfer J et al. *Surf. Sci.* **454 – 456** 885 (2000)
110. Hänke T et al. *Phys. Rev. B* **72** 085453 (2005)
111. Hänke T et al. *Phys. Rev. B* **71** 184407 (2005)
112. Schmid M et al. *Phys. Rev. Lett.* **82** 355 (1999)
113. Muzzall D E, Chiang S *Mater. Res. Soc. Symp. Proc.* **619** 57 (2000)
114. Takakuwa Y, in *MRS Spring Meeting 2002, June 18 – 21, 2002, Symp. I* "*Synchrotron Radiation and Materials Science*", I/p. 67
115. Lyapin A, Dissertation, Bericht Nr. 169 (Stuttgart: Univ. Stuttgart, 2005)
116. Wertheim G K, Citrin P H *Phys. Rev. B* **38** 7820 (1988)
117. Rosengren A *Phys. Rev. B* **24** 7393 (1981)
118. Sebilleau D et al. *J. Phys. C* **21** 287 (1988)
119. Chopra D R, Hatwar T K, Smothermon L *Surf. Sci.* **169** L311 (1986)
120. Van der Veen J F et al. *Solid State Commun.* **40** 57 (1981)
121. Treglia G et al. *J. Phys. C* **14** 3463 (1981)